LOMS: interactive online software for Classical and Combinatorial Judd-Ofelt analysis with integrated database of Judd-Ofelt parameters

Jan Hrabovsky[1,*,+], **Petr Varak**[2,3,+], **and Robin Krystufek**[4,5,+]

[1]Charles University, Faculty of Mathematics and Physics, Ke Karlovu 5, 121 16 Prague, Czech Republic
[2]Department of Inorganic Chemistry, Faculty of Chemical Technology, University of Chemistry and Technology, Prague, Technicka 5, 166 28 Prague, Czech Republic
[3]Institute of Photonics and Electronics of the Czech Academy of Sciences, Chaberska 1014/57, 182 00 Prague Czech Republic
[4]Institute of Organic Chemistry and Biochemistry of the Czech Academy of Sciences, Flemingovo n. 2, Prague 6 16610, Czech Republic
[5]Department of Physical and Macromolecular Chemistry, Faculty of Science, Charles University Hlavova 8, Prague 2 12843, Czech Republic
*jan.hrabovsky@mff.cuni.cz
+these authors contributed equally to this work

ABSTRACT

The Judd-Ofelt (JO) theory, introduced by B.R. Judd and G.S. Ofelt in 1962, has been pivotal in rare-earth optical spectroscopy for over six decades, describing intra $4f \leftrightarrow 4f$ transitions with three intensity JO parameters. Subsequently, numerous fundamental and experimental studies have explored its physical origins and proposed various extensions/corrections to enhance the original model, solidifying its status as a cornerstone in rare-earth ions absorption/emission spectroscopy. This study presents a comprehensive review of the current state of JO analysis and its systematic step-by-step experimental procedure for researchers with no previous experience with JO analysis calculations. For this purpose, the LOMS (Luminescence, optical and magneto-optical software) tool was developed which allows interactive online calculation of JO parameters and radiative material characteristics of transition probabilities, branching ratios and theoretical radiative lifetimes. Obtained results may be directly compared with newly established database of JO parameters within the same web interface www.LOMS.cz. Based on the newly introduced C-JO analysis, it is also possible to identify critical absorption band combinations necessary for accurate JO analysis ensuring consistent and reliable outcomes.

Background & Summary

Rare-earth (RE) elements and especially their trivalent ions are of high relevance in both science and industry due to their unique electronic, magnetic and spectroscopic properties, which make them indispensable in various high-tech applications[1–4]. The ability of RE ions to exhibit sharp emission/absorption spectral lines in a wide spectral range has been crucial for the development of advanced optical and photonic materials, such as e.g. solid state lasers, phosphors and light-emitting diodes (LED), scintillators, detectors[2–4]. Within the industrial sector, RE ions are essential components in the manufacturing process of strong permanent magnets, which are used in electric cars, imaging devices as the screen of smartphones/computers or as catalysts in chemical reactions[1,5–7]. Furthermore, their luminescent properties are used for medical imaging as diagnostic tools, enhancing the capabilities of modern healthcare technologies[1,2,8,9]. It is therefore not surprising that the worldwide value of products containing rare-earth elements reached almost 2 trillion US dollars in 2012, nearly a 5% of the global gross national product[10,11]. Despite extensive experimental knowledge of spectroscopic properties of rare-earth ions, the correct mechanism of the strong intra $4f \leftrightarrow 4f$ electronic transitions was only understood around the mid-20th century thanks to the advances in Racah's algebra and the enhanced computational power caused by advancements in computer technology[2,12,13]. Building on these previous accomplishments, B.R. Judd[14] and G.S. Ofelt[15] independently introduced a theory in 1962 that describes the spectroscopic properties of rare-earth ions in various materials. These studies thus established the foundation for what later became known as the Judd-Ofelt (JO) theory, the first quantum-mechanical explanation of the electric dipole induced $4f \leftrightarrow 4f$ transition intensities in RE ions through the set of three JO parameters $\Omega_i (i = 2,4,6)$. The known values of JO parameters then enable the prediction of the transition probabilities, $A(J',J)$, and consequently the values of branching ratios, $\beta(J',J)$, and theoretical luminescence radiative lifetimes, ${\tau^{\mathrm{JO}}}_{\mathrm{r}}$, parameters which are crucial for designing and optimizing photonic materials and devices. The application of JO theory thus has become widespread, which can be documented by the growing number of published scientific articles since then, with over 19 000 published by the middle of the year 2024 (see Fig.1). According to works[12,13], the main research directions may be classified into three categories as (1) Fundamental JO theory: theory improvement and development of new JO parametrisation methods[2,12,13,16–18] (2) Experimental parametrisation of materials with different RE elements or various content and prepared under different synthesis/deposition conditions[19] and (3) Applications of JO theory or obtained JO parameters to the development of various models in other research fields[20,21]. It should be noted that the last two categories make up the majority of published works and primarily focus on the practical implementation of JO theory rather than its theoretical understanding. From this perspective, it is highly desirable to offer a comprehensive summary for its experimental understanding and to develop a standardized, interactive, and online-accessible tool for its calculation. The Luminescence, optics and magneto-optics software (LOMS) then provides an accessible free-to-use online and interactive tool for JO analysis calculations and JO combinatorial analysis which enables the identification of critical absorption band combinations ensuring consistent and reliable results while using a higher-than-minimum number of measured absorption bands. The www.LOMS.cz online graphical user interface (GUI) also presents first online systematically organized dynamic repository of JO parameters according to: host materials, RE ion concentrations, method of preparation, etc., which is designed for further addition of new data from other authors in the field of rare-earth ions spectroscopy.

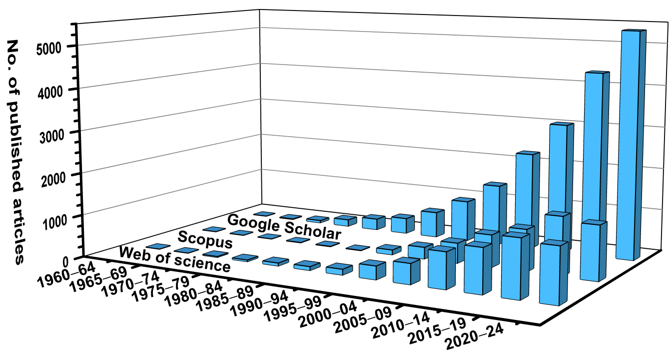

Figure 1. Tracking of "Judd-Ofelt" expression within Google Scholar, Scopus and Web of sciences (WOS) scientific databases in 5-year intervals by July 2024.

Methods

Judd-Ofelt theory: Theoretical background

To introduce JO theory and its implications, it is first necessary to define basic concepts related to the physics of rare-earth elements/ions, derivation of spectroscopic terms for RE^{3+} ground states as well as to know the position of other multiplets in energy diagram and other aspects required for in-depth spectroscopic description of solid. However, this section does not aim to provide an exhaustive mathematical treatment of JO theory and quantum mechanical descriptions, which are extensively detailed in original studies by Judd[14] and Ofelt[15] or comprehensive works by Hehlen[12] and Walsh[2]. Instead, the primary goal is to present JO theory from an experimental perspective and introduce it to the broader scientific community. Presented outcomes are then introduced in the form of the interactive free-to-use online tool (www.LOMS.cz) designed for calculating classical and combinatorial JO analysis and related parameters, facilitating accessibility and practical application of the theory. The calculated results can then be directly compared in the newly established JO parameter database on the same web platform (www.LOMS.cz/jo-database).

Rare-earth ions: spectroscopic properties and application

The Rare-earth (RE) elements consist of seventeen chemical elements in the periodic table, including fifteen lanthanides (La, Ce, Pr, Nd, Pm, Sm, Eu, Gd, Tb, Dy, Ho, Er, Tm, Yb, Lu) along with Sc and Y. While rare-earth ions typically form trivalent cations, exceptions exist where divalent (Nd^{2+}, Sm^{2+}, Eu^{2+}, Dy^{2+}, Tm^{2+}, Yb^{2+}) and quadrivalent (Ce^{4+}, Pr^{4+}, Tb^{4+}, D^{4+}) cations can also be formed. Rare-earth ions are widely used in electronics and in the production of magnets, catalysts, and photonics materials, with trivalent (RE^{3+}) cations being the most commonly utilized for these applications[1,4–7]. For this reason, the main focus will be on trivalent rare-earth cations with at least partially occupied 4f electron orbital and charge configuration of [Xe] $4f^{1-13}$. Cations with fully filled (Lu^{3+}) or empty $4f$-orbitals (La^{3+}, Y^{3+}) are not of spectroscopic interest as they do not allow any intra $4f \leftrightarrow 4f$ transitions. However, despite the lack of inherent emission bands, Y^{3+}/Lu^{3+}/La^{3+} are substantial for various applications due to their capability of host matrix formation[22]. These ions thus provide a stable and inert surrounding for other activator ions from the RE ion group, such as Nd^{3+} (Nd:YAG lasers) or Ce^{3+} (Ce:YAG/LuAG-based light emitting diodes)[1,4–7,22]. The comparable ionic radii and electronic structures allow them to form robust crystal lattices that can adopt a wide range of dopant ions to the order of tens of at.%[23]. This versatility makes them indispensable in the design of advanced phosphor materials (e.g. LED, solid state lasers), scintillators, and other luminescent materials for lighting, displays, and medical imaging technologies[1,4–7,22,23].

The primary benefit of optically active rare-earth ions with partially occupied $4f$ electron orbitals is their spectroscopic stability within the host matrix regardless of whether the matrix consists of the above-described crystalline materials with or without the Y, Lu, La content, amorphous materials or special optical glasses. Emission bands from RE^{3+} ions in the host material closely match their intrinsic energies[2,4,12], displaying narrow spectral lines and high cross sections across a broad wavelength range, from UV to MIR. In contrast, transition metals exhibit smaller cross-sections and broader spectral lines due to the significant influence of the host matrix on their 3d shells[2]. This difference occurs because the 4f shells of lanthanides are partially shielded by their outer electron shells (5s and 5p) as is visible in Table 1. This leads to a very weak interaction between these optical active electrons and the host matrix/surrounding ligand field. Perturbation of the local surrounding environment then affects the free RE^{3+} ion Hamiltonian (H_F) and leads to the creation of Stark levels. The Hamiltonian of free RE^{3+} ion can be expressed using Eq.1 as

$$H_F = H_0 + H_C + H_{SO}, \tag{1}$$

where the first term, H_0, represents the nucleus-electron interaction and the kinetic energies of all the electrons, the second term is the coulombic repulsion between electrons, H_C, and the last term describes the spin-orbit interaction, H_{SO}, and thus coupling between the spin angular momentum and the orbital angular momentum. Previously mentioned interaction with the surrounding crystal/ligand field could then be expressed by adding another term representing the perturbation Hamiltonian, V_{LF}, and form the perturbated free ion Hamiltonian for an ion in the host matrix as follows $H = H_F + V_{LF}$. For a more detailed description, please follow Refs.[2,12,14,15].

Table 1. Charge configuration of RE^{3+} ions, atomic number (Z), ionic and covalent radii (taken from Ref.[24]), number of electrons in $4f$ orbital (n_e), total spin (S) and orbital (L) angular momentum , total angular momentum (J) and derived $^{2S+1}L_J$ ground spectroscopic term.

Z	Element	Symbol	ER^{3+} config.	Ionic radius (Å)	Covalent radius (Å)	n_e	S	L	J	Ground term
58	Cerium	Ce	$[Kr]4f^1 5s^2 5p^6$	1.02	1.65	1	0.5	3	2,5	$^2F_{5/2}$
59	Praseodymium	Pr	$[Kr]4f^2 5s^2 5p^6$	1.00	1.65	2	1	5	4	$^3H_4$
60	Neodymium	Nd	$[Kr]4f^3 5s^2 5p^6$	0.99	1.64	3	1.5	6	4.5	$^4I_{9/2}$
61	Promethium	Pm	$[Kr]4f^4 5s^2 5p^6$	0.98	1.63	4	2	6	4	$^5I_4$
62	Samarium	Sm	$[Kr]4f^5 5s^2 5p^6$	0.97	1.62	5	2.5	5	2.5	$^6H_{5/2}$
63	Europium	Eu	$[Kr]4f^6 5s^2 5p^6$	0.97	1.85	6	3	3	0	$^7F_0$
64	Gadolinium	Gd	$[Kr]4f^7 5s^2 5p^6$	0.97	1.61	7	3.5	0	3.5	$^8S_{7/2}$
65	Terbium	Tb	$[Kr]4f^8 5s^2 5p^6$	1.00	1.59	8	3	3	6	$^7F_6$
66	Dysprosium	Dy	$[Kr]4f^9 5s^2 5p^6$	0.99	1.59	9	2.5	5	7.5	$^6H_{15/2}$
67	Holmium	Ho	$[Kr]4f^{10} 5s^2 5p^6$	0.97	1.58	10	2	6	8	$^5I_8$
68	Erbium	Er	$[Kr]4f^{11} 5s^2 5p^6$	0.96	1.57	11	1.5	5	7.5	$^4I_{15/2}$
69	Thulium	Tm	$[Kr]4f^{12} 5s^2 5p^6$	0.95	1.56	12	1	5	6	$^3H_6$
70	Ytterbium	Yb	$[Kr]4f^{13} 5s^2 5p^6$	0.94	1.74	13	0.5	3	3.5	$^2F_{7/2}$

The electrostatic interaction among electrons then results in the splitting of energy levels by approximately 10^4 cm^{-1}, leading to the formation of new ^{2S+1}L energy levels separated by the same order of magnitude. Further splitting of these energy levels to new $^{2S+1}L_J$ levels occurs when spin-orbit coupling is considered. The influence of ligand field perturbations subsequently generates Stark levels, a process referred to as Stark splitting which divides each J level into $2J$+1 new Stark levels with energy separation of $\approx 10^2$ cm^{-1}. Used spectroscopic symbols describe the total spin angular momentum $S = \sum s_i$ and total orbital angular momentum $L = \sum l_i$ of electron spins s_i and orbital angular momenta l_i for a given electron configuration of RE^{3+} ion. The term symbol $^{2S+1}L_J$ of the ground state of a multi-electron atom can be found according to three (1)−(3) Hund's rules, where the lowest energy term is that which (1) has the greatest spin multiplicity and (2) the largest value of the total orbital angular momentum (at the maximum multiplicity). Spin-orbit coupling then split ^{2S+1}L terms into levels according to the

(3) subshell occupancy. If the subshell is less than half full, the lowest energy belongs to the level with the lowest total angular momentum value, $J = |L - S|$, and on the opposite, if the subshell is exactly or more than half full, the lowest energy belongs to the level with the highest total angular momentum value, $J = |L + S|$. This can be demonstrated on the example of Er^{3+} cation with electron charge configuration of $[Xe]4f^{11}$ with eleven electrons in 4f orbital, where only three are unpaired. By employing the first and second Hund's rule, the total multiplicity is equal to $S = 1.5$ and the largest total orbital angular momentum is equal to $L = 6$. Using the standard notation, the letter symbol of total orbital angular momentum L = S,P,D,F,G,H,I corresponds to L = 0,1,2,3,4,5 and 6. According to the third rule, the subshell is more than half full and thus the total angular momentum value is $J = L + S = 6 + 1.5 = 15/2$. Described procedure thus results in the construction of $^{2S+1}L_J$ ground term for erbium 3+ ion as $^4I_{15/2}$. Similar information for other RE ions is listed in Table. 1. Extended energy diagram derived from optical experiments by Dieke et al.[25] is presented in Fig.2 for the subset of $^{2S+1}L_J$ multiplets and energies up to ≈5 eV (≈40 000 cm^{-1} or ≈250 nm). Presented energy levels are placed across the wavelength range covered by commonly used spectroscopic techniques and thus covers only a low-energetic part of the energy level diagram (see Fig.2) for the complete set of $^{2S+1}L_J$ multiplets for each RE^{3+} ion, which was later completed using the theoretical calculations by Peijzel et at.[26]

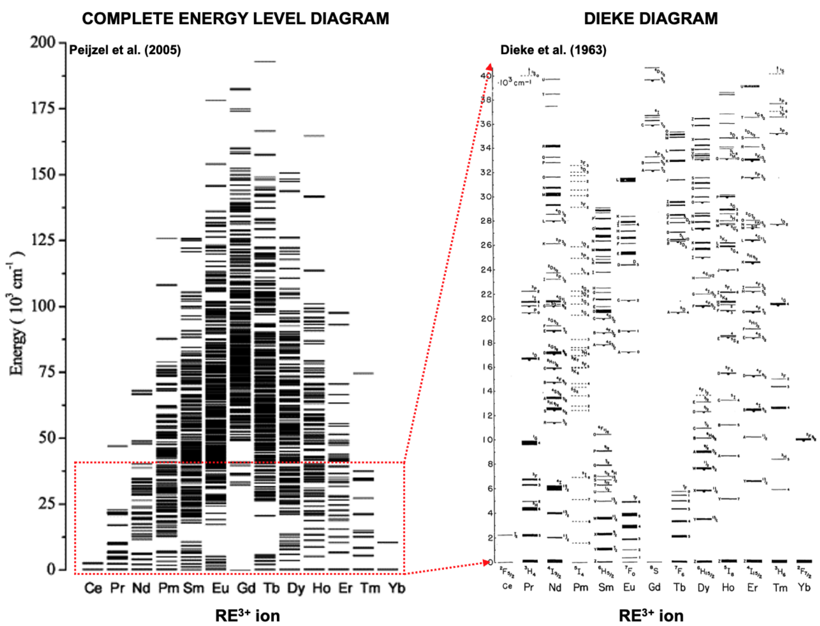

Figure 2. Energy level diagram of RE^{3+} ions for the calculated complete set of $^{2S+1}L_J$ multiplets[26] (left) and the classical experimentally determined "Dieke"[25] diagram for energies up to 40 000 cm^{-1}(right).

Judd-Ofelt theory

JO theory was introduced independently to each other by Brian R. Judd[14] and George S. Ofelt[15] in 1962 based on the previous work of J.H. Van Vleck about spectroscopic properties of rare-earth ions in solids[27]. Sharp spectroscopic lines of RE^{3+} ion implicated the intra-4f electronic transitions that occur between the levels inside the 4f electronic shell. This is, however, forbidden by the Laporte selection rule which says that states with even parity can be connected by electric dipole transitions only with states of odd parity and the same in vice versa. Among the other proposed but incorrect explanations based on (1) 4f to 5d transitions or (2) magnetic dipole or electric quadrupole radiation, Van Vleck[27] and Broer[28] presented a reasonable solution based on the distortion of the electronic motion by surrounding crystal/ligand field in the material. Presented distortions then bypass the Laporte selection rule and allow the electric dipole radiation even for intra-4f electronic transitions. However, to disturb the wavefunctions and negate the Laporte rule, the external field must also be noncentrosymmetric. From this point, about a quarter of a decade later and with further advances in algebra, computing, and increased applications of lasers, JO[14,15] theory was presented and described the induced electric dipole transitions of RE^{3+} ions in host materials.

JO theory then provides a theoretical expression for the calculation of oscillator strengths (Eq. 2), as the ratio between absorbed (emitted) and emitted (absorbed) intensity of electromagnetic radiation for harmonically oscillating electron and expresses the probability of individual J↔J' transition as follows,

$$f_{\text{theor}}(J \to J') = \frac{8\pi^2 m_e c}{3h\overline{\lambda}(2J+1)} n \left(\frac{n^2+2}{3n}\right)^2 \sum_{i=2,4,6} \Omega_i |\langle (S,L)J|U^i|J'(S',L')\rangle|^2, \tag{2}$$

where J and J' are the quantum numbers of the initial ground state and excited state, respectively, n is the refractive index, h is the Planck's constant, m_e is electron mass, c is the speed of light in vacuum, $\overline{\lambda}$ is the mean wavelength of corresponding J→J' transition and Ω_i are the JO parameters for i = 2, 4, 6. The terms in brackets are the squared reduced matrix elements, which are almost independent on the host matrix. Note, that the summation over i is also known as manifold linestrength which will be introduced later in this section. Interaction between the surrounding host matrix and RE^{3+} ions are then expressed by the set of three JO phenomenological parameters, which can be obtained by equating the expressions for the experimental (f_{exp}) and theoretical (f_{theor}) oscillator strengths using the least-squares method. The experimental oscillator strengths can be calculated from optical absorption spectra using the Eq.3,

$$f_{\text{exp}}(J \to J') = \frac{2m_e c}{\alpha_f h \overline{\lambda}^2 N} \int \alpha(\lambda) d\lambda, \tag{3}$$

where α_f is fine structure constant, N is rare-earth ion concentration and $\alpha(\lambda)$ is wavelength-dependent absorption coefficient. Optical absorption can be also expressed using the absorption cross section, σ_{abs}, defined as $\sigma_{\text{abs}} = \alpha(\lambda)/N$.

Using knowledge of the JO parameters, several important spectroscopic quantities can be calculated for a specific material system, such as the transition probabilities, $A(J',J)$, radiative lifetimes, ${\tau^{\text{JO}}}_{\text{r}}$, or the luminescence branching ratios, $\beta(J',J)$. The transition probabilities for each transition are calculated from Eq. 4:

$$A(J' \to J) = \frac{64\pi^4 e^2}{3h\lambda_B^3(2J'+1)} \left(\chi_{\text{ED}} S_{\text{ED}} + \chi_{\text{MD}} S_{\text{MD}}\right), \tag{4}$$

where J' is the total angular momentum of the upper excited state, λ_B is the transition wavelength (also called Barycenter), S_{ED} and S_{MD} are electric and magnetic dipole line strengths and χ_{ED} and χ_{MD} are the local field corrections of the electric dipole (Eq.5) and the local field correction of the magnetic dipole (Eq.6).

$$\chi_{\text{ED}} = n \left(\frac{n^2+2}{3}\right)^2, \tag{5}$$

$$\chi_{\text{MD}} = n^3, \tag{6}$$

The electric dipole linestrength is then easily calculated from each excited state manifold to lower lying manifold using the JO parameters and matrix elements by Eq. 7:

$$S_{\text{ED}} = \sum_{i=2,4,6} \Omega_i |\langle (S,L)J|U^i|J'(S',L')\rangle|^2, \tag{7}$$

where e is unit charge of electron. The magnetic dipole line strengths are given by Eq. 8:

$$S_{\text{MD}} = \left(\frac{h}{4\pi m_e c}\right)^2 |\langle (S,L)J|\hat{L} + g\hat{S}|J'(S',L')\rangle|^2, \tag{8}$$

where g is the electron g-factor (g≈ 2.002) and the terms in brackets are reduced matrix elements of the $|L+gS|$ operator. The radiative lifetimes of each level, ${\tau^{\text{JO}}}_{\text{r}}$, are then calculated from the transition probabilities using Eq.9. The luminescence branching ratio, $\beta(J',J)$ is given by Eq.10 and represents the distribution of the emission transitions in the emission spectra. Combining the theoretical JO lifetime and branching ratio with the experimentally measured lifetime, τ_{r}, for a designated transition results in Eq.11, which defines the radiative quantum yield, η, of the corresponding $J' \to J$ electronic transition.

$${\tau^{\text{JO}}}_{\text{r}} = \frac{1}{\sum_{J'} A(J',J)}, \tag{9}$$

$$\beta(J',J) = \frac{A(J',J)}{\sum_{J'} A(J',J)}, \tag{10}$$

$$\eta(J',J) = \frac{\tau_{\rm r}}{\tau^{\rm JO}{}_{\rm r}}\beta(J',J), \tag{11}$$

The quality of the least-squares fit can be quantified by the $\sigma_{\rm RMS}$ parameter, expressed by Eq. 12:

$$\sigma_{\rm rms} = \sqrt{\frac{\sum(f_{\rm exp} - f_{\rm theor.})^2}{T-3}}, \tag{12}$$

where T is the number of transitions used for the calculation.

Judd-Ofelt theory: Experimental practice

From the experimental perspective, accurate spectroscopic characterization of the prepared materials is essential for the proper application of the JO theory and estimation of JO parameters, transition probabilities and derived values of branching ratios and theoretical luminescence lifetimes.

The first step of the JO analysis requires the measurement of the transmission spectrum, $T(\lambda)$, to determine the wavelength-dependent values of the absorption coefficient, $\alpha(\lambda)$, and then the values of the absorption cross-section, $\sigma_{\rm abs}(\lambda)$. Although the calculation of the $\sigma_{\rm abs}(\lambda)$ value from the absorption coefficient using the known RE^{3+} ion concentration (N) is relatively simple, where $\sigma_{\rm abs}(\lambda) = \alpha_{\rm k}(\lambda)/N$, the calculation of the absorption coefficient may vary across the literature depending on whether scattering losses are not included (13), included (14) and if taking into account multiple reflections in plane parallel geometry of the sample (15) (in the case of solids). As is visible from Fig.3 in the example of Er^{3+}-doped glass, the spectral shape of corresponding transitions in the transparent region is practically identical with significant offset caused by the not included/included reflectivity (R). In cases where the absorption band is offset from the zero $\sigma_{\rm abs}(\lambda)$ value or overlaps with the absorption edge, it is therefore necessary to subtract the background to obtain the most possible accurate value. If the number of observed manifolds is sufficient, it is recommended to exclude the transitions within the absorption edge from the calculation of the JO parameters to increase fit accuracy.

$$\alpha_1 = \frac{-1}{l} ln(T) = \frac{-2.303 log_{10}(T)}{l} \tag{13}$$

$$\alpha_2 = \frac{-1}{l} ln\left(\frac{T}{(1-R)^2}\right) = \frac{2.303\left[-log_{10}(T) + log_{10}(1-R)^2\right]}{l} \tag{14}$$

$$\alpha_3 = \frac{1}{l} ln\left[\frac{(1-R)^2 + \sqrt{(1-R)^4 + 4R^2T^2}}{2T}\right] \tag{15}$$

Derived spectral dependence of the $\sigma_{\rm abs}(\lambda)$ is used for estimation of the integrated absorption cross section, $\int_{J\to J'} \sigma_{\rm abs}(\lambda) d\lambda$ (in cm^2 nm), for each manifold (Fig.3b) which is then used for calculation of the experimental oscillator strength (Eq.3) or experimental linestrength (Eq.16) according to

$$S_{\rm exp}(J \to J') = \frac{3ch(2J+1)}{8\pi^3 e^2 \bar{\lambda}} n \left(\frac{3}{n^2+2}\right)^2 \int_{J\to J'} \sigma(\lambda) d\lambda, \tag{16}$$

where J is the quantum number representing the total angular momentum of the original ground state, found from the ${}^{2S+1}L_J$ term constructed by using the three Hund's rules (see previous section for detailed description). As the linestrength is typically referred in cm^2, the units and input values for other quantities and constants in presented calculations are used as follows: speed of light, $c = 3 \times 10^{10}$cm s^{-1}, Planck constant, $h = 6.626 \times 10^{-30}$ cm^2 kg s^{-1}, unit charge of electron, $e = 1.5189 \times 10^{-11}$ cm$^{3/2}$ kg$^{1/2}$ s^{-1}, fine structure constant, $\alpha = 7.297 \times 10^{-3} \approx 1/137$, and electron mass, $m_{\rm e} = 9.11 \times 10^{-11}$kg. The last presented parameter, mean wavelength ($\overline{\lambda}$), can be found as well from the absorption cross section data using the harmonic, $\overline{\lambda}_H$ (Eq.17a), or weighted mean value, $\overline{\lambda}_W$ (Eq.17b), for each transition as is illustrated in Fig.3b. Both derived mean values lead to almost similar results, which, however, may differ from the value of simply subtracting absorption band maximum, λ_{max}. Note, that for the proper calculation of experimental oscillator strength or experimental linestrength, the values of experimentally determined integrated cross section and mean wavelength must be recalculated after subtraction from the graph and used in (cm^2 cm) and (cm), respectively.

$$\text{(a) } \overline{\lambda}_H = \frac{1}{\frac{\sum \lambda \sigma_{abs}(\lambda)}{\sum \sigma_{abs}(\lambda)}} = \frac{\sum \sigma_{abs}(\lambda)}{\sum \lambda \sigma_{abs}(\lambda)} \text{ or (b) } \overline{\lambda}_W = \frac{\sum \sigma_{abs}(\lambda)\lambda}{\sum \sigma_{abs}(\lambda)} \tag{17}$$

By completing all of the above characteristics, the JO phenomenological parameters, $\Omega_i (i = 2, 4, 6)$ are determined by fitting the experimental absorption represented by experimental oscillator strength (Eq.3) or linestrength (Eq.16) using the least square method to the theoretical ones described via Eq.(2) or Eq.(7). On the example of the second case, experimental and theoretical linestrengths are written in their respective matrix forms similarly as described in Ref.[2] and the sum of the square difference is minimized. Since the JO theory includes only three parameters, more than three absorption manifolds have to be provided for calculation, and thus JO theory cannot be applied to single Yb^{3+}-doped materials. After fitting procedure, materials characteristics, such as $A(J',J), \beta(J',J)$ and $\tau^{JO}{}_r$, are calculated using the known JO parameters from Eq.4, Eq.9 and Eq.10. Nevertheless, for proper calculation of transition probabilities (Eq.4), it is also necessary to know the value of corresponding transition ($J' \rightarrow J$) wavelength from an excited state to the ground/lower-energy state, λ_B, also commonly referred as Barycenter. This value should be in principle different from the mean wavelength $\overline{\lambda}$ or absorption band maximum (λ_{max}). However, the assignment of the barycenter varies considerably within the literature (or is not clearly explained) and can be divided into three main approaches, using the (1) similar value of mean wavelength $\overline{\lambda}$ derived from the optical absorption measurements as Barycenter or (2) tabulated values assigned with U^2,U^4,U^6 elements regardless of the host material or (3) the peak/mean wavelength derived from emission spectra at room temperature. Using the last approach, it is possible to estimate the spectral shift between mean absorption and emission wavelength for one transition and then apply this difference to all other transitions. Given the extensive nature of the topic, it is up to the author which approach is chosen and which would best fit the experimental results.

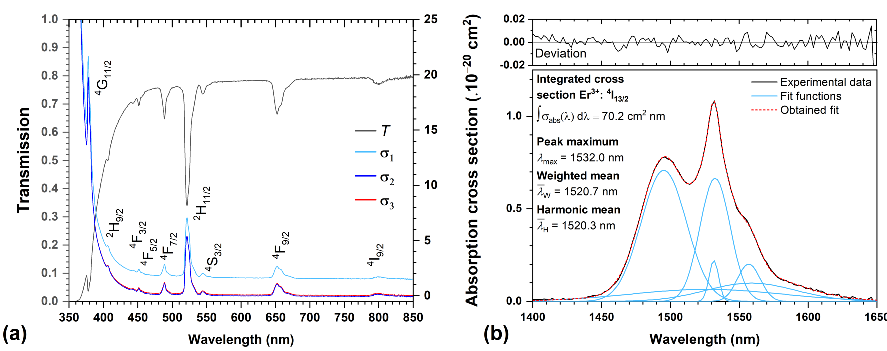

Figure 3. a) Transmission spectrum and corresponding absorption cross sections, employing various corrections on scattering losses or plane parallel geometry of the sample; b) example of integrated area calculation of a selected band.

Combinatorial Judd-Ofelt theory

Following the previous section, it is clear that the selection of the appropriate transition bands and their experimental description is crucial for accurate calculation of the JO parameters[2,12,29]. To compute the JO parameters, at least four experimentally measured absorption manifolds must be used. When a larger set of measured absorption bands is available, it becomes possible to exclude certain transitions (e.g., those exhibiting hypersensitivity) or to limit the JO analysis to transitions within a specific spectral region, for example, due to experimental limitations or the presence of fundamental absorption of the host matrix. However, for accurate determination of the complete set of all three JO parameters, the following criteria must be met: (1) the involved transitions must have non-zero values of the corresponding reduced squared matrix elements U^i $(i = 2, 4, 6)$, (2) these values should be of the same order of magnitude, and (3) at least three transitions that satisfy the previous two conditions must be used.

As a result, various studies exclude hypersensitive transitions, such as the $^2H_{11/2}$ transition for Er^{3+} ions with a high U^2 value, do not cover the full spectral range due to the lack of experimental capability to measure absorption bands in the NIR/MIR regions (Nd^{3+} ($^4I_{11/2}$), Dy^{3+} ($^6H_{13/2}$), Sm^{3+} ($^6H_{7/2}$ and $^6H_{9/2}$), etc) or selectively include/exclude transitions affected by the absorption edge. This last scenario can be particularly limiting for materials with low optical transmission in the visible spectral region, such as chalcogenide glasses, since this region typically contains the majority of experimentally observable absorption bands associated with rare-earth ions. For some materials, it is therefore in principle necessary to include the transitions affected by the absorption edge, otherwise they would not meet the condition for the minimum number of used manifolds. Using Combinatorial Judd-Ofelt analysis (C-JO)[29] and a higher than minimum number of transitions, it is thus possible to identify those manifold combinations that enable accurate JO analysis ensuring consistent and reliable results. Moreover, by employing various types of host materials and broad-spectrum analysis for each eare-earth ion it will be possible to identify such critical combinations, which are essential for the calculation of JO parameters and thus should not be omitted. The total value of all possible combinations then depends on the number of input absorption bands (N_B) according to Eq.18

$$\text{Total combinations} = \sum_{r=k}^{N_B} \binom{N_B}{r} \tag{18}$$

,

where k is the minimum number of elements in each combination (from 4 to N_B) and $\binom{N_B}{r}$ is the binomial coefficient calculated as $\binom{N_B}{r} = \frac{N_B!}{r!(N_B-r)!}$. It is then possible to obtain 5, 22, 64, 163, 382 and 848 possible combinations for original sets composed of 5, 6, 7, 8, 9 and 10 experimentally obtained absorption bands. The obtained set of all possible combinations can be subsequently reduced by inappropriate combinations using different empirical approaches (e.g. due to unphysicality of partial solutions or non-converging results when calculating JO parameters) or using the analysis of statistical distribution of the resulting JO parameter values depending on the absorption bands used[29]. In order to eliminate the empirical selection approach, the box/whisker plot statistical method may be applied to the original set of all possible combinations reduced by the non-physical cases (negative values of JO parameters)[29]. According to the used statistical model, data points (combinations) outside the whisker boundaries are identified as outliers and thus may be excluded from the dataset as was shown in Ref.[29] on the example of Er^{3+}-doped materials. Several other examples of presented C-JO analysis are given in the following section *Technical Validation:Judd-ofelt analysis and Combinatorial Judd-Ofelt analysis*.

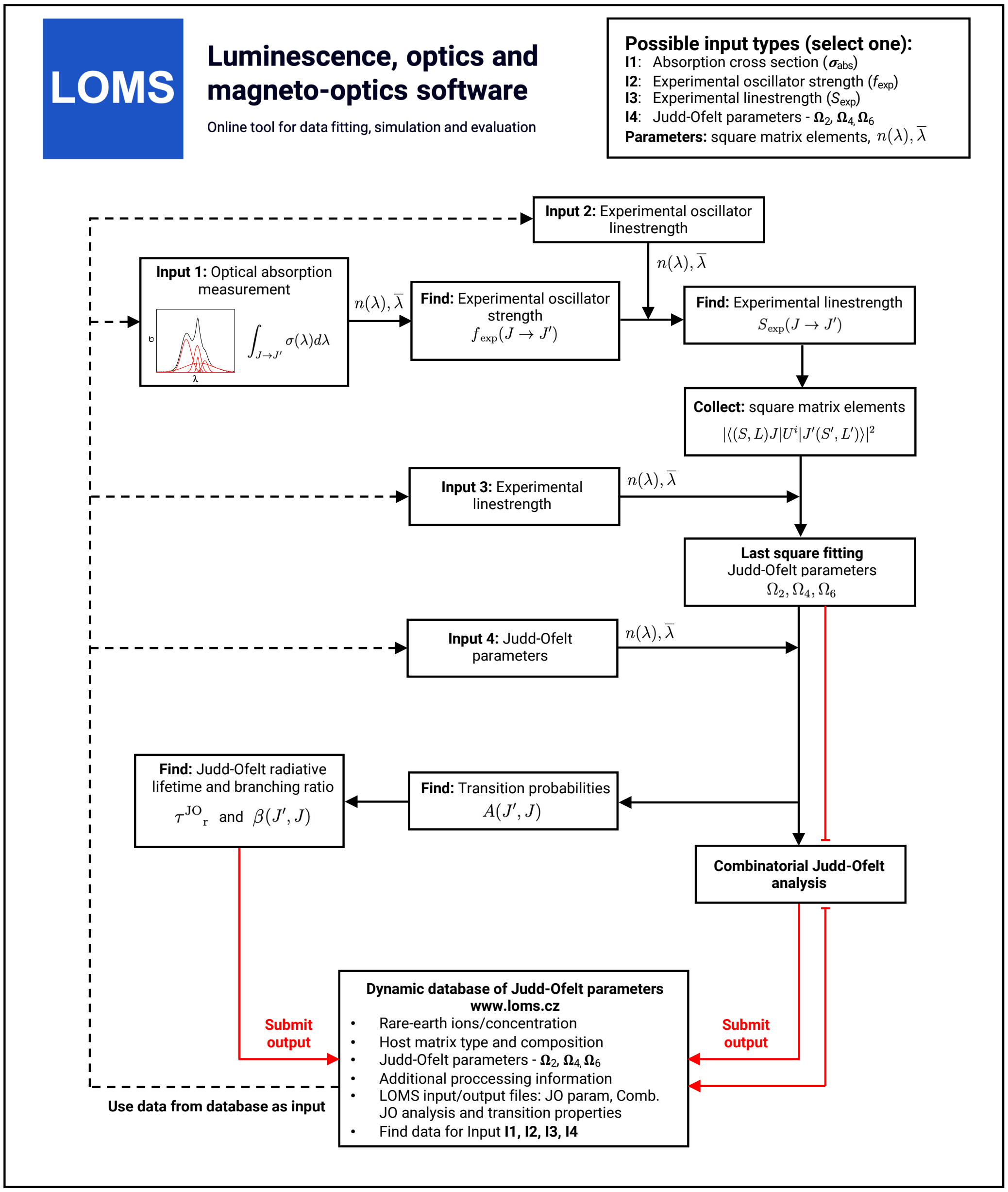

Figure 4. Software procedure of Judd-Ofelt analysis and implementation of Judd-Ofelt parameters database.

Usage Notes: Graphical software interface

The process of JO and Combinatorial JO analysis using the Luminescence, optics and magneto-optics software (LOMS) (www.LOMS.cz) is captured in the attached flowchart (Fig.4) and the GUI of LOMS software is shown in Fig.5. To enhance versatility, users can select from four recommended input options based on the desired level of data processing/verification (Fig.5, Radio button: *Input values*). The capability for direct processing of experimental oscillator strength/linestrength input data was implemented to facilitate potential comparison with experimental data in the literature. Furthermore, the possibility of direct input of JO parameters and subsequent calculation of material radiative characteristics has been added. The list of possible input files is as follows:

1. Integrated absorption cross section $\int \sigma_{\text{abs}} d\lambda$ (in cm^2 nm) or
2. Experimental oscillator strength, f_{exp}, taken from an external source or calculated using Eq.3 or
3. Experimental linestrength, S_{exp} (in cm^2), taken from an external source or calculated using Eq.16 or
4. Judd-Ofelt parameters, $\Omega_2, \Omega_4, \Omega_6$, (in cm^2), taken from an external source or calculated using aforementioned procedure.

Furthermore, to successfully calculate JO parameters and radiation material characteristics (transition probabilities, radiative lifetimes and branching ratios), the input file must be supplemented with the following data sets for each experimentally derived manifold:

1. Refractive index (Fig.5, Radio button: *Refractive index values*) and
2. Mean peak wavelength (in nm) derived using Eq.17 for each placed transition (Fig.5, Text field: *Mean peak wavelength*)
3. Square matrix elements U^2, U^4, U^6 for each placed transition (Fig.5, Text fields: *U2, U4, U6*)
4. Barycenter: (in cm^{-1}) for each transition. If they are not experimentally detectable, it is necessary to use their tabulated values or choose one of the approaches discussed further in this section (Fig.5, Text fields: *Barycenter*).

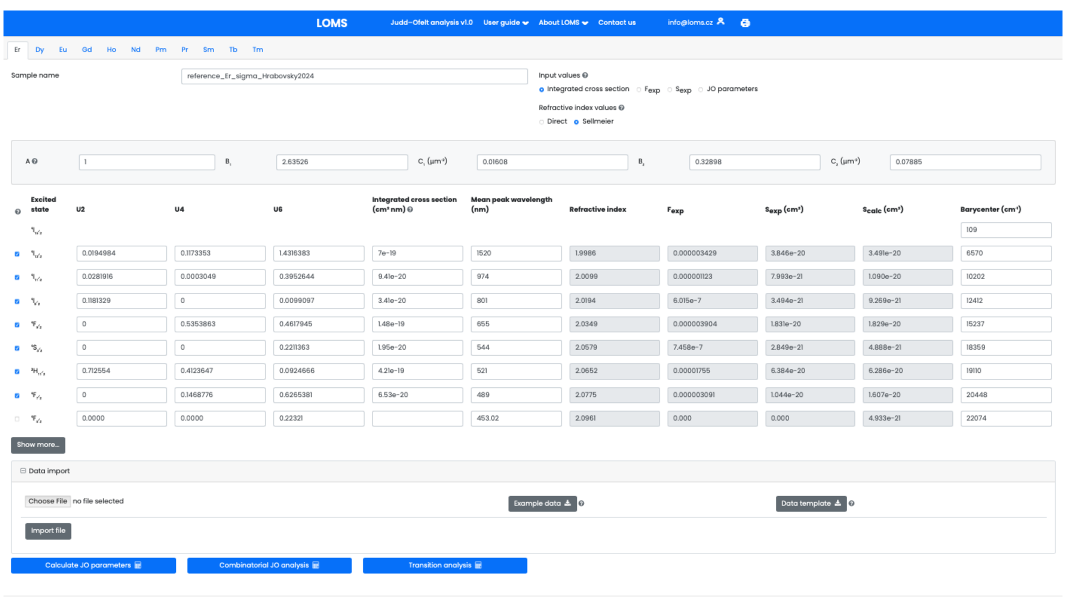

Figure 5. The graphical user interface of LOMS online tool, which is available at https://www.LOMS.cz/.

The refractive index can be added directly as defined values for each transition in the same row (Fig.5, Text field: *Refractive index*) or expressed using a standard two-term Sellmeir model (Eq.19)

$$n^2 = A + \frac{B_1 \lambda^2}{\lambda^2 - C_1} + \frac{B_2 \lambda^2}{\lambda^2 - C_2}, \tag{19}$$

where the A, B_1, C_1, B_2 and C_2 are the Sellmeier coefficients. Note, that while it is possible to directly enter the refractive index values (sufficient for calculation of JO parameters), calculating the radiation characteristics, $A(J',J), \beta(J',J)$ and $\tau^{\mathrm{JO}}{}_{\mathrm{r}}$, requires inputting its spectral dependence via the specified Sellmeier coefficients. If the refractive index of the material is not directly available, it can be obtained from one of the accessible material databases, such as *refractiveindex.info*[30]. A consistent set of tabulated matrix elements for all RE elements listed in Table 1 and default values of barycenters and mean peak wavelengths are provided (see Figshare repository[31] or www.LOMS.cz) with the possibility of their interactive editing in the software GUI if necessary. An important added functionality is also the possibility to interactively select the number of involved transitions (column of checkboxes on the left side in Fig.5) without the need to change/modify the input data structure. Once all the above requirements have been met, the classical JO analysis can be calculated via pressing button *Calculate JO parameters* and complete combinatorial JO analysis for all possible combinations of inserted absorption bands can be performed by pressing the *Combinatorial JO analysis*. The results structure in GUI is shown in Fig.6.

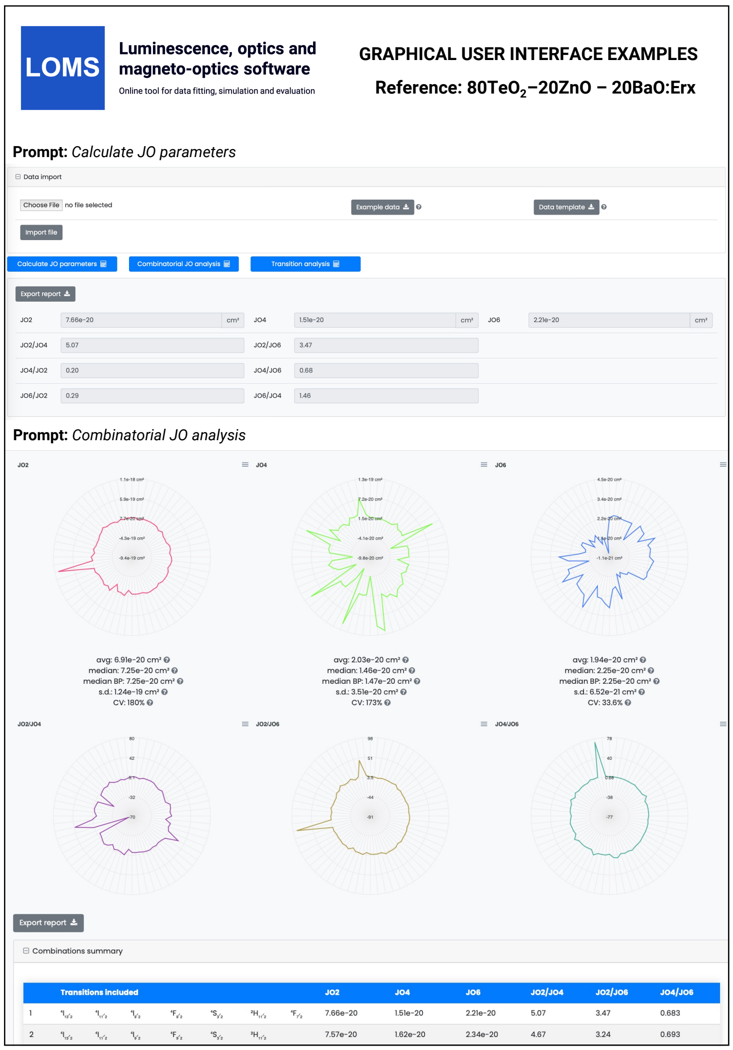

Figure 6. The graphical user interface of LOMS online tool (https://www.LOMS.cz.): Illustrative example of results structure for classical and combinatorial Judd-Ofelt analysis.

Note, that in many cases, two or more closely located transitions may overlap with each other and therefore it is not possible to easily distinguish their independent contribution. This can be the example of two absorption bands $^2H_{11/2}$ ($\approx$ 530 nm) and $^4S_{3/2}$ ($\approx$ 550 nm) in Er^{3+}-doped materials. In such cases, it is therefore necessary to apply a modified procedure for the calculation of JO parameters as follows: (1) estimate the combined integrated absorption cross section which involves both absorption bands, (2) estimate the mean peak wavelength in the same way as if it was a single absorption band, (3) sum the respective matrix elements of all the participating transitions into one and (4) write them to the LOMS.cz online GUI in one line - choose the line of one of the involved transitions (or similarly in input .csv file). This modified procedure then affects the U2, U4, U6, integrated cross section and mean wavelength cells. For better clarity, the difference is visible in Fig.(7) and the data repository[31] also contains .xls reference file with shown calculation process. It is also important to note, that it is necessary to uncheck the remaining transitions so that only the one combined transition/row participates in the calculation. This then acts as the combined level of $^2H_{11/2} + ^4S_{3/2}$. It is then necessary to remember that in the output file of the JO analysis and the combinatorial JO analysis, this transition no longer represents only one level, but a combination of all involved manifolds. However, this no longer applies to the calculation of radiative transitions properties (A, β, τ), which is done separately and independently of whether the combined or single bands were used for the calculation of JO parameters or not. This is of course due to the fact that radiative properties are calculated directly from the JO parameters, i.e. energy level assignment in *Transition analysis* section is independent of the structure of the data input.

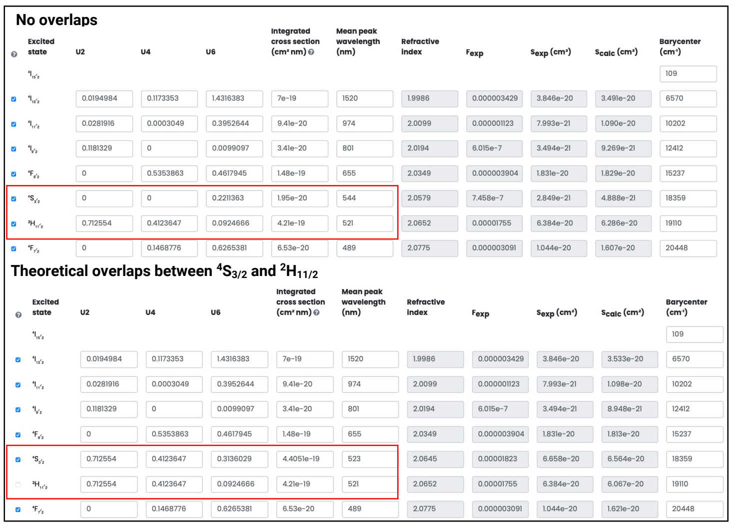

No overlaps

	Excited state	U2	U4	U6	Integrated cross section (cm^2 nm)	Mean peak wavelength (nm)	Refractive index	F_{exp}	S_{exp} (cm^2)	S_{calc} (cm^2)	Barycenter (cm^{-1})
	$^4I_{15/2}$										109
☑	$^4I_{13/2}$	0.0194984	0.1173353	1.4316383	7e-19	1520	1.9986	0.000003429	3.846e-20	3.491e-20	6570
☑	$^4I_{11/2}$	0.0281916	0.0003049	0.3952644	9.41e-20	974	2.0099	0.000001123	7.993e-21	1.090e-20	10202
☑	$^4I_{9/2}$	0.1181329	0	0.0099097	3.41e-20	801	2.0194	6.015e-7	3.494e-21	9.269e-21	12412
☑	$^4F_{9/2}$	0	0.5353863	0.4617945	1.48e-19	655	2.0349	0.000003904	1.831e-20	1.829e-20	15237
☑	$^4S_{3/2}$	0	0	0.2211363	1.95e-20	544	2.0579	7.458e-7	2.849e-21	4.888e-21	18359
☑	$^2H_{11/2}$	0.712554	0.4123647	0.0924666	4.21e-19	521	2.0652	0.00001755	6.384e-20	6.286e-20	19110
☑	$^4F_{7/2}$	0	0.1468776	0.6265381	6.53e-20	489	2.0775	0.000003091	1.044e-20	1.607e-20	20448

Theoretical overlaps between $^4S_{3/2}$ and $^2H_{11/2}$

	Excited state	U2	U4	U6	Integrated cross section (cm^2 nm)	Mean peak wavelength (nm)	Refractive index	F_{exp}	S_{exp} (cm^2)	S_{calc} (cm^2)	Barycenter (cm^{-1})
	$^4I_{15/2}$										109
☑	$^4I_{13/2}$	0.0194984	0.1173353	1.4316383	7e-19	1520	1.9986	0.000003429	3.846e-20	3.533e-20	6570
☑	$^4I_{11/2}$	0.0281916	0.0003049	0.3952644	9.41e-20	974	2.0099	0.000001123	7.993e-21	1.098e-20	10202
☑	$^4I_{9/2}$	0.1181329	0	0.0099097	3.41e-20	801	2.0194	6.015e-7	3.494e-21	8.948e-21	12412
☑	$^4F_{9/2}$	0	0.5353863	0.4617945	1.48e-19	655	2.0349	0.000003904	1.831e-20	1.813e-20	15237
☑	$^4S_{3/2}$	0.712554	0.4123647	0.3136029	4.4051e-19	523	2.0645	0.00001823	6.658e-20	6.564e-20	18359
☐	$^2H_{11/2}$	0.712554	0.4123647	0.0924666	4.21e-19	521	2.0652	0.00001755	6.384e-20	6.067e-20	19110
☑	$^4F_{7/2}$	0	0.1468776	0.6265381	6.53e-20	489	2.0775	0.000003091	1.044e-20	1.621e-20	20448

Figure 7. The graphical user interface of LOMS online tool, with shown comparison between data input structure without and with observed absorption band overlap. See the main text for discussion.

Results of transition analysis, calculation of $A(J', J), \beta(J', J), \tau^{JO}{}_r, A_{(ED)}, A_{MD}$, will be displayed after pressing the *Transition analysis* button (see Fig.5). The results structure for radiative transition analysis in GUI is shown in Fig.8 and the structure of example output file is visible from Table2. Note, that for successful transition analysis, it is also necessary to include the Barycenter values for each transition and not only for those which were inserted. It is because the transition probabilities, $A(J', J)$ (Eq.4), are calculated for each transition ($J' \rightarrow$J) from an excited state to the ground/lower-energy state. As was discussed in the section *Judd-Ofelt theory: Experimental practice*, the barycenter value should be in principle different from the mean wavelength $\overline{\lambda}$ or absorption band maximum (λ_{max}) as the position of photoluminescence emission is usually red-shifted compared to position of optical absorption (this is valid for both peak/mean wavelength values). However, the assignment of the barycenter varies considerably within the literature (or is not clearly explained) and can be divided into three main approaches, using the (1) similar value of mean wavelength $\overline{\lambda}$ derived from the optical absorption measurements as Barycenter or (2) tabulated values assigned with U^2,U^4,U^6 elements regardless of the host material or (3) the peak/mean wavelength derived from emission spectra at room temperature. To avoid limiting of the calculation, the software allows all the above-mentioned options depending on the selected value. The LOMS.cz software then calculates the energy difference between selected energy levels, which will be used for the calculation of transition probabilities (Eq.4). The barycenter values may be then inserted as follows:

1. **Barycenter value similar to mean wavelength:** (1) leave the first box for the ground state in Barycenter column (Fig.5,Text fields: *Barycenter*) blank or equal to zero, (2) fill the other positions with corresponding recalculated values of mean wavelength in cm^{-1} (cm^{-1} = 10^7/nm)

2. **Tabulated values of Barycenter:** fill the corresponding manifold cell for each transition using the tabulated values.

3. **Barycenter value with the constant shift:** according to software procedure (JOFwin2011) presented by Walsh[2], it is possible to insert the offset position of the ground state which more or less represents the energy spectral shift between optical absorption and emission band peak/mean maximum. In this case, the value in the first box for the ground state in Barycenter column contains the value of this energy spectral shift, whereas the other values represents the mean wavelengths (in cm^{-1}) derived from optical absorption spectra.

Using the last approach, it is possible to estimate the spectral shift between mean absorption and emission wavelength for one transition and then apply this difference to all other transitions. Given the extensive nature of the topic, it is up to the author which approach is chosen and which would best fit the experimental results.

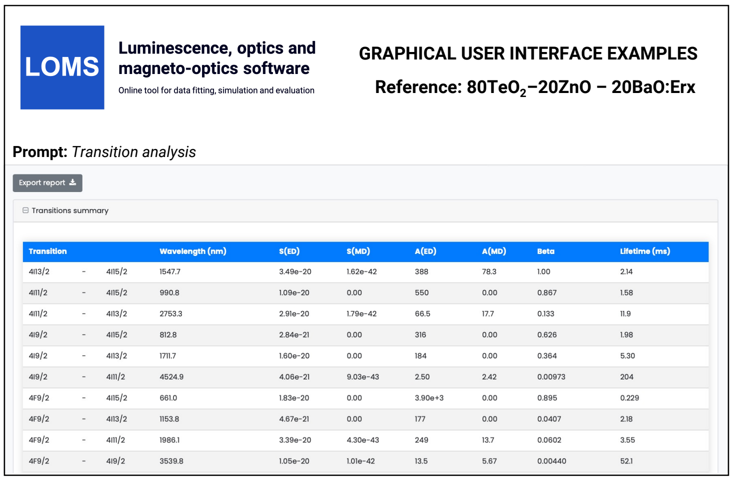
LOMS
Luminescence, optics and magneto-optics software
Online tool for data fitting, simulation and evaluation

GRAPHICAL USER INTERFACE EXAMPLES
Reference: $80TeO_2$–20ZnO – 20BaO:Erx

Prompt: *Transition analysis*

Export report

Transitions summary

Transition			Wavelength (nm)	S(ED)	S(MD)	A(ED)	A(MD)	Beta	Lifetime (ms)
4I13/2	-	4I15/2	1547.7	3.49e-20	1.62e-42	388	78.3	1.00	2.14
4I11/2	-	4I15/2	990.8	1.09e-20	0.00	550	0.00	0.867	1.58
4I11/2	-	4I13/2	2753.3	2.91e-20	1.79e-42	66.5	17.7	0.133	11.9
4I9/2	-	4I15/2	812.8	2.84e-21	0.00	316	0.00	0.626	1.98
4I9/2	-	4I13/2	1711.7	1.60e-20	0.00	184	0.00	0.364	5.30
4I9/2	-	4I11/2	4524.9	4.06e-21	9.03e-43	2.50	2.42	0.00973	204
4F9/2	-	4I15/2	661.0	1.83e-20	0.00	3.90e+3	0.00	0.895	0.229
4F9/2	-	4I13/2	1153.8	4.67e-21	0.00	177	0.00	0.0407	2.18
4F9/2	-	4I11/2	1986.1	3.39e-20	4.30e-43	249	13.7	0.0602	3.55
4F9/2	-	4I9/2	3539.8	1.05e-20	1.01e-42	13.5	5.67	0.00440	52.1

Figure 8. The graphical user interface of LOMS online tool (https://www.LOMS.cz.): Illustrative example of results structure for *Transition analysis*

Data Records

The complete set of blank template input files for each rare-earth ion, illustrative examples of input files together with attached results for JO and C-JO analysis and dataset of JO parameters listed in LOMS.cz database is available at Figshare[31] or the www.LOMS.cz webpage.

It presently, as of August 2024, contains:

1. **Template files:** complete set of eleven templates for Pr^{3+}, Nd^{3+}, Pm^{3+}, Sm^{3+}, Eu^{3+}, Gd^{3+}, Tb^{3+}, Dy^{3+}, Ho^{3+}, Er^{3+} and Tm^{3+} trivalent rare-earth ions which contains: identification of $J \to J'$ transition with associated values of reduced matrix elements, mean-wavelenghts and barycenters obtained from Walsh[2] JOFwin2011 documentation as a reference.

2. **Reference files:** example set of reference files with different types (I.−IV. of inputs, Fig.4) for JO analysis, C-JO analysis and calculation of radiative properties of Pr^{3+}[32], Nd^{3+}[33], Pm^{3+}[34], Sm^{3+}[35,36], Tb^{3+}[37], Dy^{3+}[38,39], Ho^{3+}[40,41], Er^{3+}[29,42] and Tm^{3+}[43,44] trivalent rare-earth ions

3. **Combinatorial Judd-Ofelt analysis:** output files from C-JO analysis for RE^{3+}-doped materials which contains JO parameters of all possible combinations of involved measured intre-4f transitions

4. **Database of Judd-Ofelt parameters:** 1228 data records of JO parameters and resulting radiative properties for 12 RE^{3+} ions on 585 materials/host matrices of various compositions[19,29,32–34,36–296].

Structure of .csv file import

To standardize and simplify the data upload process, users can utilize the option to upload the required data via a .csv file, using the provided templates for all elements. The template .csv file for each RE^{3+} ion is unique and cannot be exchanged between each other since it contains the corresponding absorption transitions notation, assigned square matrix elements, etc. To successfully complete the form, the following steps must be completed:

1. **Template file:** Download the template file on the relevant rare-earth ion page (www.LOMS.cz/jo) or module documentation (www.LOMS.cz/modules/judd-ofelt-analysis/) or from Figshare data repository[31]

2. **Refractive index import:** Enter the refractive index input structure in the appropriate field following the *ref_index_type* cell (see Fig.9) as (1) *sellmeier* for input via Eq.19 or (2) *direct* for direct refractive index input. Based on your selection, enter either the Sellmeier coefficients or refractive index values for the corresponding transitions in the column labelled "refractive_index."

3. **Transitions and Square matrix elements:** verify/replace the tabulated square matrix elements but do not change the labels of the individual transitions in the first column.

4. **Input type:** Select the corresponding form of your input type as follows: absorption cross section (*sigma*), experimental oscillator strength (*fext*), experimental linestrength (*sexp*) or JO parameters (*jo*) and write it down to the cell named *input_date* (rewrite it). The input values for corresponding transitions have to be placed in the same column. For the selection of JO parameters as an input (only for calculation of radiative properties), please insert the $\Omega_2, \Omega_4, \Omega_6$ JO parameters to the U^2, U^4, U^6 of the ground state (replace the zero values).

5. **Mean peak wavelength:** Enter the mean peak wavelengths for the transitions for which input data has been provided (see the previous text for proper estimation of mean wavelength value).

6. **Barycenter:** Check or provide relevant data for all transitions, otherwise it will not be possible to calculate the relevant radiation characteristics. Please see *Usage Notes: Graphical software interface* section for more details regarding the proper barycenter selection.

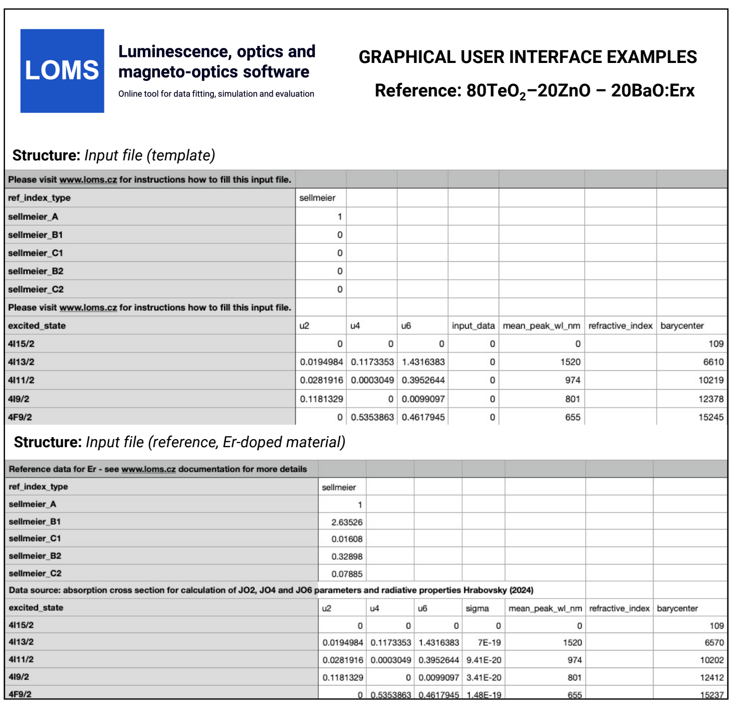

Please visit www.loms.cz for instructions how to fill this input file.							
ref_index_type	sellmeier						
sellmeier_A	1						
sellmeier_B1	0						
sellmeier_C1	0						
sellmeier_B2	0						
sellmeier_C2	0						
Please visit www.loms.cz for instructions how to fill this input file.							
excited_state	u2	u4	u6	input_data	mean_peak_wl_nm	refractive_index	barycenter
4I15/2	0	0	0	0	0		109
4I13/2	0.0194984	0.1173353	1.4316383	0	1520		6610
4I11/2	0.0281916	0.0003049	0.3952644	0	974		10219
4I9/2	0.1181329	0	0.0099097	0	801		12378
4F9/2	0	0.5353863	0.4617945	0	655		15245

Reference data for Er - see www.loms.cz documentation for more details							
ref_index_type	sellmeier						
sellmeier_A	1						
sellmeier_B1	2.63526						
sellmeier_C1	0.01608						
sellmeier_B2	0.32898						
sellmeier_C2	0.07885						
Data source: absorption cross section for calculation of JO2, JO4 and JO6 parameters and radiative properties Hrabovsky (2024)							
excited_state	u2	u4	u6	sigma	mean_peak_wl_nm	refractive_index	barycenter
4I15/2	0	0	0	0	0		109
4I13/2	0.0194984	0.1173353	1.4316383	7E-19	1520		6570
4I11/2	0.0281916	0.0003049	0.3952644	9.41E-20	974		10202
4I9/2	0.1181329	0	0.0099097	3.41E-20	801		12412
4F9/2	0	0.5353863	0.4617945	1.48E-19	655		15237

Figure 9. The structure of import .csv file.

Structure of .csv output file

Calculated results of JO analysis, Combinatorial JO analysis and radiative transition properties can be exported in the form of .csv files upon clicking on the button *Export report* in the corresponding section (see Fig.6 and Fig.8). Example output files for the mentioned references are included in Figshare repository[31] and correspond to the data structrures presented in Fig.6 and Fig.8. Data export from classical JO analysis also contains all input information for selected bands and both experimental and theoretical values of linestrength accompanied by the estimated ratios between calculated JO parameters.

Technical Validation: Judd-Ofelt analysis and Combinatorial Judd-Ofelt analysis

The general procedure of JO analysis, radiative transition analysis and C-JO analysis is shown in a flow chart in Fig.4 using four different input types: I. integrated cross section, II. experimental oscillator strength, III. experimental linestrength and IV. Judd-Ofelt parameters. Technical aspects and major steps in the process are described in the sections *Judd-Ofelt theory: Experimental practice* and *Usage Notes: Graphical software interface*. The validity of the presented procedures is then presented in the following text on the examples of materials doped with Er^{3+}[29,42], Dy^{3+}[38,39], Ho^{3+}[40,41], Nd^{3+}[33], Pm^{3+}[34], Pr^{3+}[32], Sm^{3+}[35,36], Tb^{3+}[37] and Tm^{3+}[43,44] ions. Furthermore, C-JO analysis is provided for materials with more than four observed separate transitions, which allows the investigation of the most consistent and reliable outcomes using various combinations of absorption bands for JO analysis. Reference input files for all mentioned RE^{3+}-doped materials are included in Figshare data repository[31] together with a complete set of output files. The Combinatorial JO analysis results for selected RE^{3+} ions are presented within this text only in graphic form (Fig.10−13) due to the high number of possible combinations, where for 5, 6, 7, 8, 9, 10, 11, 12 and 13 experimentally observed input manifolds, it is possible to calculate 6, 22, 64, 163, 382, 848, 1816, 3797 and 8514 mutual manifolds combinations. Complete step-by-step procedure is presented here for the first reference of $TeO_2-ZnO-BaO$ tellurite glass doped with Er^{3+} ions (TZB:Er)[29]. Other references are presented in shorter form concerning calculated JO parameters and results of the Combinatorial JO analysis (see Table3).

The Er-doped material ($TeO_2-ZnO-BaO$ glass) was chosen as the main example due to the presence of a reasonable number (seven observed manifolds) of absorption bands across the optical transmission spectral window when some of them may overlap with each other. The visible part of the absorption spectrum of TZB:Er glass is shown in Fig.3. Derived dependency of baseline corrected absorption cross section was used to obtain the integral in Eq.16, which represents the integrated cross section (sum over the wavelength) for each observed manifold. These experimentally determined values were used as *Input type I* in the LOMS.cz software accompanied by the positions of mean wavelength and refractive index value for each manifold to calculate the experimental linestrengths values, which were used for JO fitting. Figshare data repository also contains other possible input types formats for this material, where *Input type II:* experimental oscillator strength, *Input type III:* experimental linestrength and *Input type IV:* JO parameters respectively. The last input type can be used together with known refractive index spectral dependency only for calcualtion of radiative properties. The placement of matrix elements (U^2, U^4, U^6), integrated cross section, mean wavelength and both experimental and theoretical linestrength values within LOMS.cz GUI interface is shown in Fig.5. The JO parameters were found to be $\Omega_2 = 7.66\times10^{-20}\text{cm}^2$, $\Omega_4 = 1.51\times10^{-20}\text{cm}^2$ and $\Omega_6 = 2.21\times10^{-20}\text{cm}^2$ which is in agreement with values presented in Ref.[29] and values obtained by fitting procedure using the Walsh[2] evaluation software JOFwin(2011), where $\Omega_2 = 7.651\times10^{-20}\text{cm}^2$, $\Omega_4 = 1.508\times10^{-20}\text{cm}^2$ and $\Omega_6 = 2.208\times10^{-20}\text{cm}^2$. The JO parameters were then used to calculate the transition probabilities according to Eq.4 between any excited state and any lower-lying energy level and to calculate the branching ratios and radiative lifetimes. The obtained results are shown in Fig.8 and Table 2. Note, that the data structure in Table 2 is similar to the format of output file generated by LOMS online tool. The calculated values were again compared to those in Ref.[29] and calculated using JOFwin2011[2] software with a good agreement. It is thus possible to verify the validity and accuracy of JO analysis fitting procedure and calculation of radiative properties. To further verify the validity of LOMS.cz software calculations, a similar procedure was applied to other materials doped with RE^{3+} ions using different data Input types and various number of observed manifolds. Calculated results are listed in Table3 with corresponding references and denoted number of used manifolds in the parentheses. The presented results are in good agreement with the associated reference values and possible deviations are caused by the use of different values of matrix elements, used constants and parameters or minor deviations in the calculation of linestrength values across the literature.

The reference datasets with more than four manifolds were used for providing C-JO analysis and investigation of results consistency as the function of involved absorption bands in the calculation of JO parameters. The Table 3 then contains the median values (Median) obtained from the set of all possible combinations and box-plot median values (Median BP)[29] obtained from the statistically reduced set of possible combinations which can be compared to the values of JO parameters calculated using the maximum possible number of observed manifolds (Full.set). Graphical results of C-JO analysis are shown in Fig.(10−13). The complete output files are included in Figshare repository[31] for detailed inspections.

Table 2. Calculated Judd-Ofelt radiative transition properties in TZB:Er glass using LOMS.cz online tool (in similar format as the software output file). The Transition eState represent the initial excited state (J'), Transition gState represent the final ground/lower lying state (J), λ_{em} is the emission wavelength calculated as the difference between involved energy levels which positions is represented by insterted values of Barycenters, S(ED) and S(MD) are electric and magnetic dipole line strengths and their respective contributions to the electric and magnetic transition probabilities A(ED) and A(MD), β is the branching ration and last two columns represent the calculated values of radiative lifetime using the LOMS.cz online tool and those taken from Ref.[29].

Transition eState	Transition gState	λ_{em} (nm)	S(ED) (cm^2)	S(MD)	A(ED) (s^{-1})	A(MD)	β	$\tau^{JO}{}_r$ (LOMS) (ms)	$\tau^{JO}{}_r$ (Ref.[29])
4I13/2	4I15/2	1547.7	3.49×10^{-20}	1.62×10^{-42}	388	78.3	1.00	2.14	2.15
4I11/2	4I15/2	990.8	1.09×10^{-20}	0.00	550	0.00	0.867	1.58	1.58
4I11/2	4I13/2	2753.3	2.91×10^{-20}	1.79×10^{-42}	66.5	17.7	0.133	11.9	11.9
4I9/2	4I15/2	812.8	2.84×10^{-21}	0.00	316	0.00	0.626	1.98	1.98
4I9/2	4I13/2	1711.7	1.60×10^{-20}	0.00	184	0.00	0.364	5.30	5.30
4I9/2	4I11/2	4524.9	4.06×10^{-21}	9.03×10^{-43}	2.50	2.42	0.00973	204	204
4F9/2	4I15/2	661.0	1.83×10^{-20}	0.00	3.90×10^{3}	0.00	0.895	0.229	0.230
4F9/2	4I13/2	1153.8	4.67×10^{-21}	0.00	177	0.00	0.0407	2.18	2.18
4F9/2	4I11/2	1986.1	3.39×10^{-20}	4.30×10^{-43}	249	13.7	0.0602	3.55	3.56
4F9/2	4I9/2	3539.8	1.05×10^{-20}	1.01×10^{-42}	13.5	5.67	0.00440	52.1	52.1
4S3/2	4I15/2	547.9	4.89×10^{-21}	0.00	4.77×10^{3}	0.00	0.683	0.143	0.144
4S3/2	4I13/2	848.2	7.65×10^{-21}	0.00	1.87×10^{3}	0.00	0.268	0.452	0.453
4S3/2	4I11/2	1225.9	1.70×10^{-21}	0.00	134	0.00	0.0192	2.92	2.92
4S3/2	4I9/2	1681.5	6.81×10^{-21}	0.00	206	0.00	0.0295	4.79	4.80
4S3/2	4F9/2	3203.1	5.88×10^{-22}	0.00	2.55	0.00	0.000366	392	392
2H11/2	4I15/2	526.3	6.29×10^{-20}	0.00	2.33×10^{4}	0.00	0.953	0.0408	0.0409
2H11/2	4I13/2	797.4	3.85×10^{-21}	3.26×10^{-43}	380	138	0.0212	0.873	0.874
2H11/2	4I11/2	1122.6	5.64×10^{-21}	1.17×10^{-43}	194	17.4	0.00864	1.59	1.60
2H11/2	4I9/2	1493.0	2.32×10^{-20}	2.19×10^{-44}	336	1.37	0.0138	2.41	2.41
2H11/2	4F9/2	2582.0	2.82×10^{-20}	2.54×10^{-44}	78.1	0.306	0.00320	12.7	12.8
2H11/2	4S3/2	13315.6	3.23×10^{-21}	0.00	0.0649	0.00	0.00000265	1.54×10^{4}	1.54×10^{4}
4F7/2	4I15/2	491.7	1.61×10^{-20}	0.00	1.12×10^{4}	0.00	0.838	0.0746	0.0747
4F7/2	4I13/2	720.6	5.09×10^{-21}	0.00	1.03×10^{3}	0.00	0.0772	0.461	0.462
4F7/2	4I11/2	976.0	7.62×10^{-21}	0.00	604	0.00	0.0450	0.883	0.884
4F7/2	4I9/2	1244.4	1.21×10^{-20}	1.61×10^{-43}	458	26.3	0.0361	1.89	1.89
4F7/2	4F9/2	1919.0	1.78×10^{-21}	5.46×10^{-43}	18.1	24.1	0.00315	22.0	22.0
4F7/2	4S3/2	4787.0	9.27×10^{-23}	0.00	0.0603	0.00	0.00000450	311	311
4F7/2	2H11/2	7473.8	1.85×10^{-20}	0.00	3.16	0.00	0.000236	316	317

Table 3. Comparison of the Judd–Ofelt parameters Ω_i (i = 2; 4; 6) for various materials with denoted number of involved manifolds for JO analysis in parenthesis. Calculated JO parameters were obtained using all experimentally measured manifolds (Full.set) or as a median value from a complete set (Median) or reduced set (by Box plot method - Median BP) of possible combinations calculated using Combinatorial Judd-Ofelt analysis.

RE^{3+}	Host matrix	Involved transitions	Ω_2	Ω_4 ($\times 10^{-20} cm^2$)	Ω_6	Reference
Er^{3+}	$80TeO_2-20ZnO-20BaO$ (glass)	Full.set (7)	7.66	1.51	2.21	Hrabovsky (2024)[29] and This work
		Median	7.25	1.46	2.25	
		Median BP	7.25	1.47	2.25	
	Ge_{25}-$Ga_{9.5}Sb_{0.5}S_{65}$ (glass)	Full.set (4)	4.31	2.46	1.96	Strizik (2014)[42]
		Full.set (4)	4.31	2.46	1.96	This work
Dy^{3+}	YVO_4 (single crystal)	Full.set (8)	6.59	3.71	1.74	Cavalli (2002)[38]
		Full.set (8)	6.56	3.6	1.76	This work
		Median	6.39	3.17	2.05	
		Median BP	6.55	3.6	2.05	
	$\alpha-KGd(WO_4)_2$	Full.set (13)	15.347	3.053	2.006	Kaminskii (2002)[39]
		Full.set (13)	15.7	2.72	2.12	This work
		Median	14.9	3.05	2.61	
		Median BP	14.8	3.08	2.53	
Ho^{3+}	$LiYF_4$ (single crystal)	Full.set (13)	1.03	2.32	1.93	Walsh (1998)[41]
		Full.set (13)	1.03	2.31	1.94	This work
		Median	1.08	2.22	1.93	
		Median BP	1.11	2.21	1.93	
	$Y_3Al_5O_{12}$ (single crystal)	Full.set (12)	0.101	2.086	1.724	Walsh (2006)[40]
		Full.set (12)	0.102	2.08	1.73	This work
		Median	0.105	2.06	1.69	
		Median BP	0.171	2.06	1.69	
Nd^{3+}	Y_2O_3	Full.set (9)	3.1728	3.0819	1.9825	Walsh (2002)[33]
		Full.set (9)	3.17	3.09	1.99	This work
		Median	3.17	3.06	1.92	
		Median BP	3.19	3.02	1.92	
Pm^{3+}	65PbO-$20P_2O_5$-$6In_2O_3$ (glass)	Full.set (7)	3.8	2.4	2.6	Shinn (1988)[34]
		Full.set (7)	3.74	2.45	2.68	This work
		Median	3.82	2.34	2.66	
		Median BP	3.82	2.33	2.66	
Pr^{3+}	$RbPb_2Cl_5$	Full.set (7)	10.63	9.22	3.72	Merkle (2017)[32]
		Full.set (7)	10.8	8.99	3.82	This work
		Median	10.7	8.99	3.82	
		Median BP	10.8	8.99	3.82	
Tb^{3+}	$LiTbF_4$	Full.set (13)	1.5	2.23	2.06	Vasyliev (2013)[37]
		Full.set (13)	1.51	2.23	2.06	This work
		Median	1.07	2.69	1.67	
		Median BP	1.52	2.46	1.68	
Sm^{3+}	Sr_2SiO_4	Full.set (6)	0.52	0.284	0.398	Manjunath (2018)[35]
		Full.set (6)	0.573	0.282	0.399	This work
		Median	0.521	0.283	0.413	
		Median BP	0.521	0.293	0.413	
	TeO_2BiCl_3 (glass)	Full.set (7)	0.48	2.04	1.83	Boudchica (2023)[36]
		Full.set (7)	0.476	2.11	1.95	this work
		Median	0.5	2.25	1.91	
		Median BP	0.964	2.29	1.89	
Tm^{3+}	GeO_2–BaO/CaO–Na_2O/Li_2O (glass)	Full.set (6)	6.14	1.54	0.87	Walsh (2006)[43]
		Full.set (6)	6.22	1.49	1.22	This work
		Median	6.37	1.57	1.22	
		Median BP	6.37	1.55	1.22	
	$Sr_5(PO_4)_3F$ (S-FAP crystal)	Full.set (4)	7.633	10.48	3.281	Bonner (2006)[44]
		Full.set (4)	7.63	10.5	3.28	This work

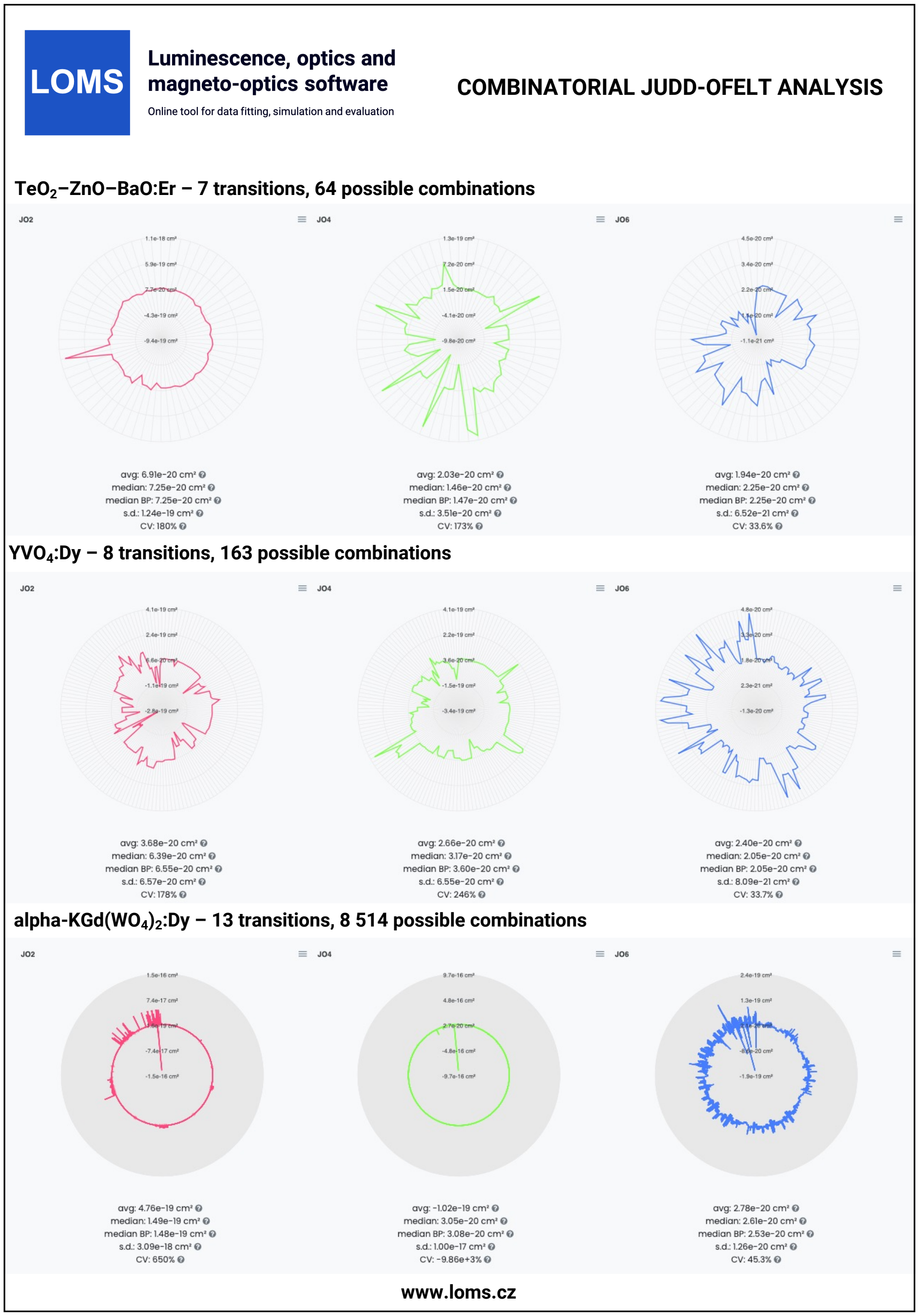

Figure 10. Technical validation examples of combinatorial Judd-Ofelt analysis for materials doped with Er^{3+} and Dy^{3+} ions. Complete data outputs are listed in Figsahere repository[31]

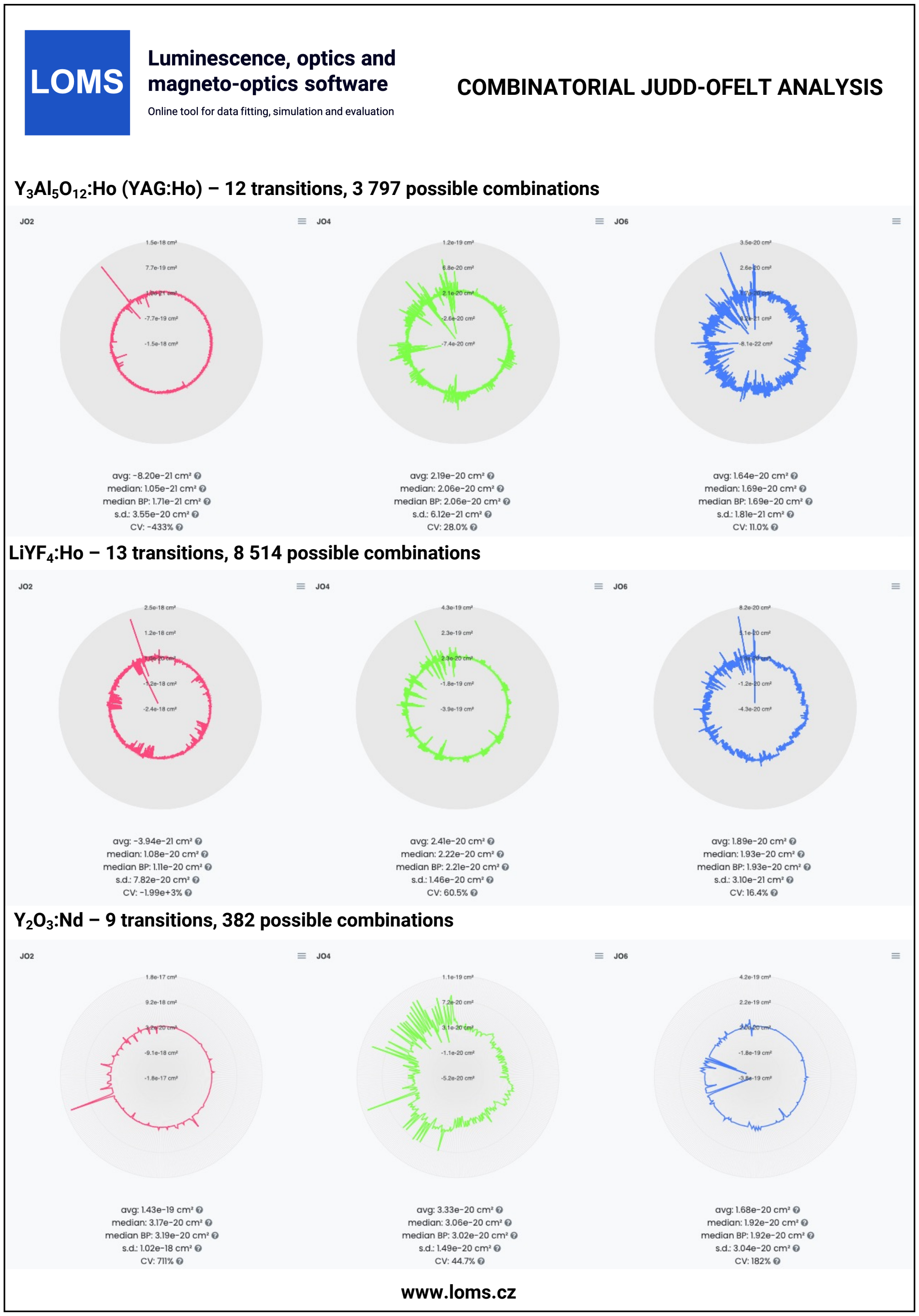

Figure 11. Technical validation examples of combinatorial Judd-Ofelt analysis for materials doped with Ho^{3+} and Nd^{3+} ions. Complete data outputs are listed in Figsahere repository[31]

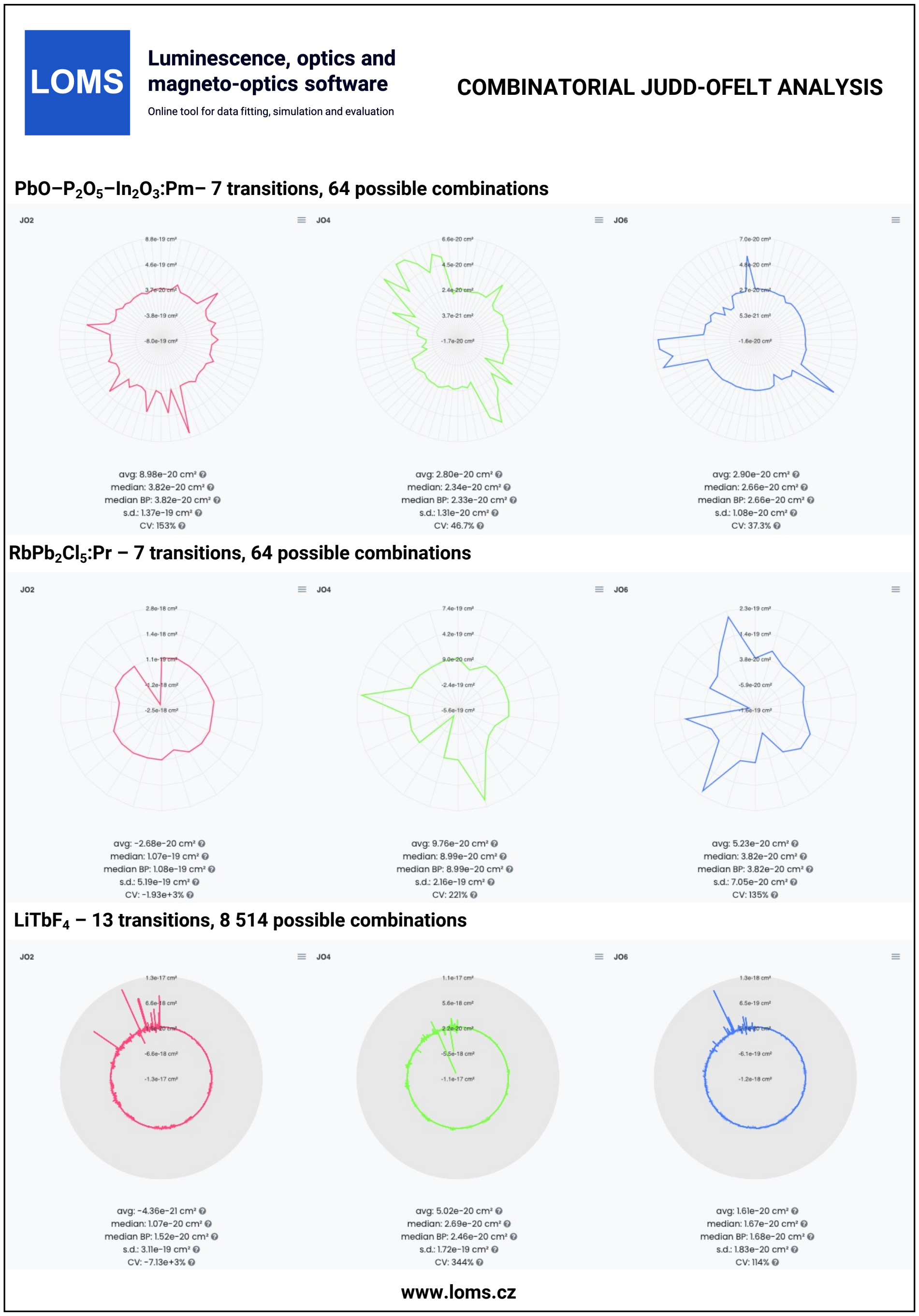

Figure 12. Technical validation examples of combinatorial Judd-Ofelt analysis for materials doped with Pm^{3+}, Pr^{3+} and Tb^{3+} ions. Complete data outputs are listed in Figsahere repository[31]

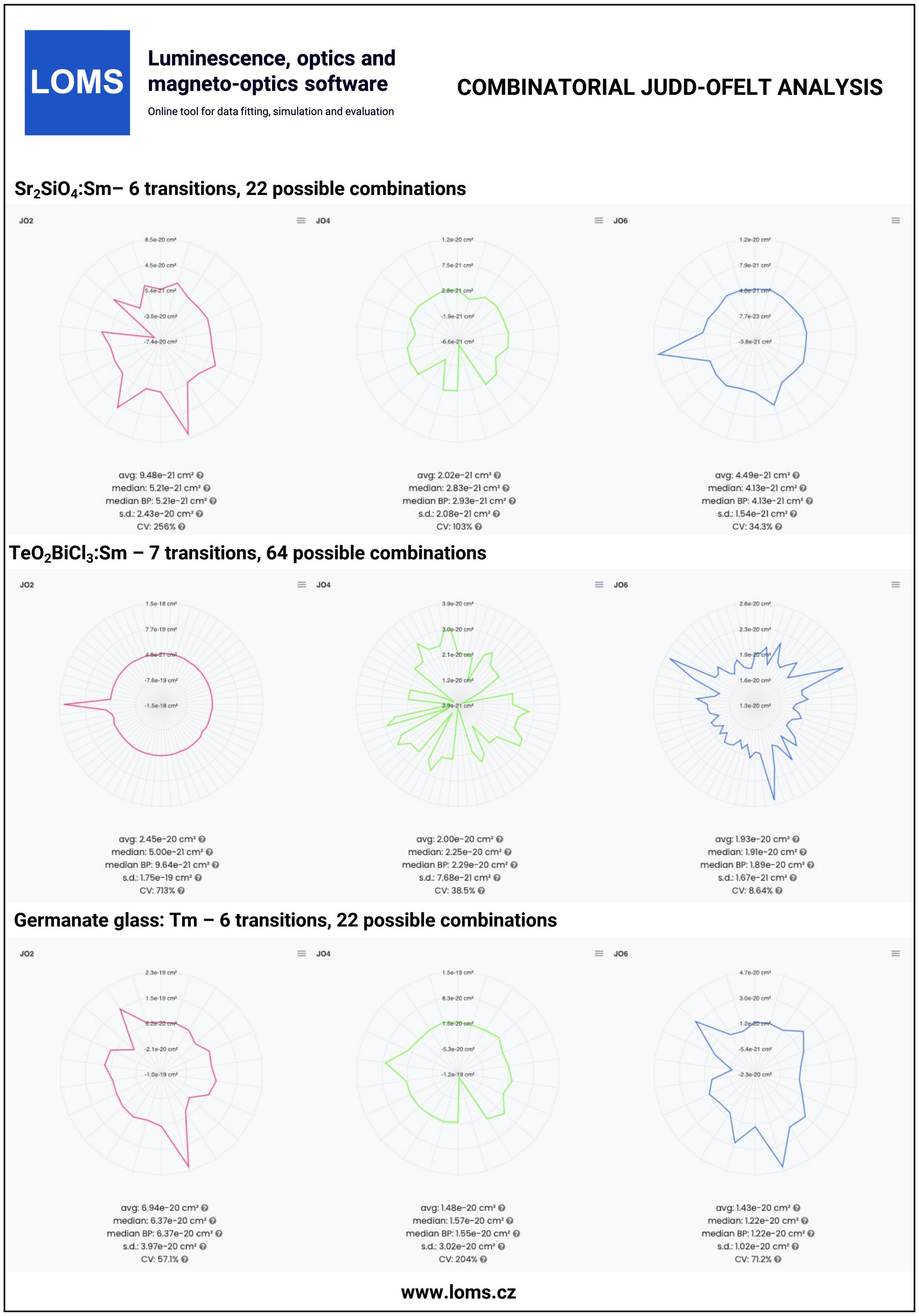

Figure 13. Technical validation examples of combinatorial Judd-Ofelt analysis for materials doped with Sm^{3+} and Tm^{3+} ions. Complete data outputs are listed in Figshare repository[31]

Technical Validation:JO paramaters database

As a logical extension of the LOMS.cz program for JO parameters calculation, a database of JO parameters was created, which allows fast dynamic reading of JO parameters and the ability to attach input and output files from the program.

Presented database of JO parameters and associated information is readable regarding the composition of the host matrix, implemented rare-earth ion/ions, RE^{3+} ions concentration, method of preparation, etc. Given that this dataset encompasses a vast collection of data compiled by numerous researchers over more than six decades, it was not feasible to verify the accuracy of each individual record. Instead, reliance was placed on the peer-review processes employed by scientific journal reviewers/publishers and their expertise and reputation. However, meticulous attention is given to ensuring the precision of data extraction and conversion processes, as well as maintaining the consistency of the information included in the dataset. Typically, the following steps are involved in adding a new data record:

1. **Verification of data source:** only peer-reviewed materials were accepted which contains DOI, ISSN or ISBN number
2. **Data origin:** each data record was traced to the first trustable publication accompanied by one of the above mentioned identifiers. This identifiers is then included in the *Reference* field within the database.
3. **Additional information:** each entry is accompanied by a set of further infomation regarding the concentration of RE^{3+} ions and its chemical form (oxide, halide, metal,..), state of host matrix (single crystal, polycrystal, glass, solution, etc.), method of preparation, etc.
4. **Duplicity check:** each new data record was check for duplicity in combination of rare-earth ion and used host matrix to avoid similar data entries.
5. **LOMS files:** selected data records were reevaluated using the LOMS online tool to confirm both their accuracy and the usability of the LOMS software (see Table3). If so, the complete set of input and output files is attached in the Figshare data repository[31] and in the *LOMS file* field within the database.

Code availability

The complete set of blank template input files for each rare-earth ion, illustrative examples of input files together with attached results for JO and C-JO analysis and dataset of JO parameters listed in LOMS.cz database is available at Figshare[31] or the https://www.LOMS.cz/ webpage. The JO parameter database contains 1228 data records of JO parameters and radiative properties for 12 different RE^{3+} ions and 585 types of materials/host matrices of various compositions.

The LOMS.cz Software is licensed for personal, classroom, education and internal use only and not for the benefit of a third party (https://www.LOMS.cz/about/). The entire software codebase is publicly available on the LOMS.cz GitHub project (https://github.com/robinkrystufek/LOMS-JO). Presented repository of JO parameters is regularly updated to meet the ongoing scientific or industrial/engineering needs. Note that the data included in the JO parameters database and utilized in template/reference files are sourced from publicly available, peer-reviewed publications, such as scientific journals and handbooks/databooks. This curation ensures their reliability, and thus, their factual accuracy has not been further independently verified. Every data entry in the dataset or/and reference/template file clearly references its source which can be found in the following reference list[19,29,32–34,36–296], allowing users to explore the original data and its further context. The Luminescence, Optics, and Magneto-Optics software (www.LOMS.cz) thus stands out as a vital resource by offering a user-friendly online tool for JO as well as C-JO analysis, and providing a comprehensive database of JO parameters in a standardized file format. With regular updates and open access, it proves indispensable for researchers, engineers, and students investigating the complex spectroscopic properties of rare-earth-doped materials.

References

1. Wybourne, B. The fascination of the rare earths—then, now and in the future. *J. Alloy. Compd.* **380**, 96–100, 10.1016/j.jallcom.2004.03.034 (2004).
2. Walsh, B. Judd-Ofelt theory: principles and practices. *Di Bartolo, B., Forte, O. (eds) Adv. Spectrosc. for Lasers Sens.* https://doi.org/10.1007/1-4020-4789-4_21 (2006).
3. Zhou, B., Li, Z. & Chen, C. Global potential of rare earth resources and rare earth demand from clean technologies. *Minerals* **7**, 10.3390/min7110203 (2017).
4. Liu, G. & (eds), B. J. *Spectroscopic Properties of Rare Earths in Optical Materials* ((Springer 2005), 2005).
5. Zhou, B., Li, Z., Zhao, Y., Zhang, C. & Wei, Y. Rare earth elements supply vs. clean energy technologies: new problems to be solve. *Gospodarka Surowcami Miner. - Miner. Resour. Manag.* **32**, 10.1515/gospo-2016-0039 (2016).

6. Gutfleisch, O. *et al.* Magnetic materials and devices for the 21st century: Stronger, lighter, and more energy efficient. *Adv. Mater.* **23**, 821–842, 10.1002/adma.201002180 (2011).

7. Sagawa, M., Fujimura, S., Togawa, N., Yamamoto, H. & Matsuura, Y. New material for permanent magnets on a base of Nd and Fe (invited). *J. Appl. Phys.* **55**, 2083–2087, 10.1063/1.333572 (1984).

8. Dong, H. *et al.* Lanthanide nanoparticles: From design toward bioimaging and therapy. *Chem. Rev.* **115**, 10725–10815, 10.1021/acs.chemrev.5b00091 (2015).

9. Zhou, J., Liu, Z. & Li, F. Upconversion nanophosphors for small-animal imaging. *Chem. Soc. Rev.* **41**, 1323–1349, 10.1039/C1CS15187H (2012).

10. HCSS/TNO. *Collaboration on Rare Earth Elements. An analysis of potentials for collaboration with Japan on Rare Earths* (The Hague Centre for Strategic Studies and TNO: The Hague, Netherlands, 2012).

11. Tukker, A. Rare earth elements supply restrictions: Market failures, not scarcity, hamper their current use in high-tech applications. *Environ. Sci. & Technol.* **48**, 9973–9974, 10.1021/es503548f (2014).

12. Hehlen, M., Brik, M. & Kramer, K. 50th anniversary of the Judd–Ofelt theory: An experimentalist's view of the formalism and its application. *J. Lumin.* **136**, 221–239, 10.1016/j.jlumin.2012.10.035 (2013).

13. Ciric, A., Marciniak, L. & Dramicanin, M. Self-referenced method for the Judd–Ofelt parametrisation of the Eu^{3+} excitation spectrum. *Sci Rep* **12**, 563, 10.1038/s41598-021-04651-4 (2022).

14. Judd, B. Optical absorption intensities of rare-earth ions. *Phys. Rev.* **127**, 750–761, 10.1103/PhysRev.127.750 (1962).

15. Ofelt, G. Intensities of Crystal Spectra of Rare-Earth Ions. *The J. Chem. Phys.* **37**, 511–520, https://doi.org/10.1063/1.1701366 (1962).

16. Goldner, P. & Auzel, F. Application of standard and modified Judd–Ofelt theories to a praseodymium-doped fluorozirconate glass. *J. Appl. Phys.* **79**, 7972–7977, 10.1063/1.362347 (1996).

17. Smentek, L. *Judd-Ofelt Theory — The Golden (and the Only One) Theoretical Tool of f-Electron Spectroscopy*, chap. 10 (John Wiley Sons, Ltd, 2015).

18. Sytsma, J., Imbusch, G. & Blasse, G. The spectroscopy of Gd^{3+} in yttriumoxychloride: Judd–Ofelt parameters from emission data. *J. Chem. Phys.* **91**, 1456–1461, 10.1063/1.457106 (1989).

19. Görller-Walrand, C. & Binnemans, K. Chapter 167 spectral intensities of f-f transitions. In *Handbook on the Physics and Chemistry of Rare Earths*, 101–264, 10.1016/S0168-1273(98)25006-9 (Elsevier, 1998).

20. Ciric, A., Stojadinovic, S. & Dramicanin, M. An extension of the judd-ofelt theory to the field of lanthanide thermometry. *J. Lumin.* **216**, 116749, 10.1016/j.jlumin.2019.116749 (2019).

21. Ciric, A., Stojadinovic, S. & Dramicanin, M. Approximate prediction of the cie coordinates of lanthanide-doped materials from the judd-ofelt intensity parameters. *J. Lumin.* **213**, 395–400, 10.1016/j.jlumin.2019.05.052 (2019).

22. Hrabovský, J., Kučera, M., Paloušová, L., Bi, L. & Veis, M. Optical characterization of $Y_3Al_5O_{12}$ and $Lu_3Al_5O_{12}$ single crystals. *Opt. Mater. Express* **11**, 1218–1223, 10.1364/OME.417670 (2021).

23. Hrabovský, J. *et al.* (preprint) rapid and precise large area mapping of rare-earth doping homogeneity in luminescent materials. *Res. Sq.* 10.21203/rs.3.rs-4474095/v1 (2024).

24. Lozykowski, H. Kinetics of luminescence of isoelectronic rare-earth ions in iii-v semiconductors. *Phys. Rev. B* **48**, 17758–17769, 10.1103/PhysRevB.48.17758 (1993).

25. Dieke, G. & Crosswhite, H. The spectra of the doubly and triply ionized rare earths. *Appl. Opt.* **2**, 675–686, 10.1364/AO.2.000675 (1963).

26. Peijzel, P., Meijerink, A., Wegh, R., Reid, M. & Burdick, G. A complete 4fn energy level diagram for all trivalent lanthanide ions. *J. Sol. State Chem.* **178**, 448–453, 10.1016/j.jssc.2004.07.046 (2005).

27. Vleck, J. The puzzle of rare-earth spectra in solids. *J. Phys. Chem.* **41**, 67–80, 10.1021/j150379a006 (1937).

28. Broer, L., Gorter, C. & Hoogschagen, J. On the intensities and the multipole character in the spectra of the rare earth ions. *Physica* **11**, 231–250, 10.1016/S0031-8914(45)80009-5 (1945).

29. Hrabovsky, J. *et al.* (Preprint) Doping ability, spectroscopic characterization and combinatorial Judd-Ofelt analysis of Er-doped $TeO_2ZnOBaO$ ternary tellurite glasses. *ResearchGate* 10.13140/RG.2.2.32721.54886/1 (2024).

30. Polyanskiy, M. Refractiveindex.info database of optical constants. *Sci data* **11**, 10.1038/s41597-023-02898-2 (2024).

31. Hrabovsky, J. LOMS.cz: interactive online software for Classical and Combinatorial Judd-Ofelt analysis with integrated database of Judd-Ofelt parameters. *Figshare* doplnit (2024).

32. Merkle, L. D. & Dubinskii, M. Pr:$RbPb_2Cl_5$: temperature dependent spectra, dynamics and three-for-one excitation. *Opt. Express* **25**, 19780, 10.1364/OE.25.019780 (2017).

33. Walsh, B. M. *et al.* Spectroscopic characterization of Nd:Y_2O_3: application toward a differential absorption lidar system for remote sensing of ozone. *J. Opt. Soc. Am. B* **19**, 2893, https://doi.org/10.1364/JOSAB.19.002893 (2002).

34. Shinn, M. D., Krupke, W. F., Solarz, R. W. & Kirchoff, T. A. Spectroscopic and laser properties of Pm^{3+}. *IEEE J. Quantum Electron.* **24**, 1100–1108, 10.1109/3.232 (1988).

35. Manjunath, C. *et al.* Optical absorption intensity analysis using judd-ofelt theory and photoluminescence investigation of orange-red Sr_2SiO_4: Sm^{3+} nanopigments. *Dye. Pigment.* **148**, 118–129, 10.1016/j.dyepig.2017.08.036 (2018).

36. Boudchicha, N. *et al.* Judd-Ofelt analysis and spectroscopy study of tellurite glasses doped with rare-earth (Nd^{3+}, Sm^{3+}, Dy^{3+}, and Er^{3+}). *Mater. (Basel)* **16**, 6832, 10.3390/ma16216832 (2023).

37. Vasyliev, V., Villora, E. G., Sugahara, Y. & Shimamura, K. Judd-Ofelt analysis and emission quantum efficiency of Tb-fluoride single crystals: $LiTbF_4$ and $Tb_{0.81}Ca_{0.19}F_{42.81}$. *J. Appl. Phys.* **113**, 203508, 10.1063/1.4807649 (2013).

38. Cavalli, E., Bettinelli, M., Belletti, A. & Speghini, A. Optical spectra of yttrium phosphate and yttrium vanadate single crystals activated with Dy^{3+}. *J. Alloy. Compd.* **341**, 107–110, 10.1016/S0925-8388(02)00079-8 (2002).

39. Kaminskii, A. *et al.* Optical spectroscopy and visible stimulated emission of Dy^{3+} ions in monoclinic $\alpha-KY(WO_4)_2$ and $\alpha-KGd(WO_4)_2$ crystals. *Phys. Rev. B Condens. Matter* **65**, 10.1103/PhysRevB.65.125108 (2002).

40. Walsh, B., Grew, G. & Barnes, N. Energy levels and intensity parameters of ions in $Y_3Al_5O_{12}$ and $Lu_3Al_5O_{12}$. *J. Phys. Chem. Solids* **67**, 1567–1582, 10.1016/j.jpcs.2006.01.123 (2006).

41. Walsh, B. M., Barnes, N. P. & Di Bartolo, B. Branching ratios, cross sections, and radiative lifetimes of rare earth ions in solids: Application to Tm^{3+} and Ho^{3+} ions in $LiYF_4$. *J. Appl. Phys.* **83**, 2772–2787, 10.1063/1.367037 (1998).

42. Strizik, L. *et al.* Green, red and near-infrared photon up-conversion in Ga–Ge–Sb–S:Er^{3+} amorphous chalcogenides. *J. Lumin.* **147**, 209–215, 10.1016/j.jlumin.2013.11.021 (2014).

43. Walsh, B. M., Barnes, N. P., Reichle, D. J. & Jiang, S. Optical properties of Tm^{3+} ions in alkali germanate glass. *J. Non Cryst. Solids* **352**, 5344–5352, 10.1016/j.jnoncrysol.2006.08.029 (2006).

44. Bonner, C. *et al.* A spectroscopic and Judd–Ofelt analysis of the relaxation dynamics of Tm^{3+} in the fluorapatites, FAP, S-FAP, and B-FAP. *Opt. Mater. (Amst.)* **20**, 1–12, 10.1016/S0925-3467(02)00005-8 (2002).

45. Reisfeld, R., Eyal, M. & Jørgensen, C. Comparison of laser properties of rare earths in oxide and fluoride glasses. *J. Less-common Met.* **126**, 187–194, 10.1016/0022-5088(86)90279-1 (1986).

46. Malinowski, M., Frukacz, Z., Szuflińska, M., Wnuk, A. & Kaczkan, M. Optical transitions of Ho^{3+} in YAG. *J. Alloy. Compd.* **300-301**, 389–394, 10.1016/S0925-8388(99)00770-7 (2000).

47. Patel, D., Reddy, B. & Nash-Stevenson, S. Spectroscopic and two-photon upconversion studies of Ho^{3+}-doped $Lu_3Al_5O_{12}$. *Opt. Mater. (Amst.)* **10**, 225–234, 10.1016/S0925-3467(97)00177-8 (1998).

48. Yang, J. *et al.* Spectroscopic properties and thermal stability of erbium-doped bismuth-based glass for optical amplifier. *J. Appl. Phys.* **93**, 977–983, 10.1063/1.1531840 (2003).

49. Tanabe, S., Ohyagi, T., Soga, N. & Hanada, T. Compositional dependence of Judd-Ofelt parameters of Er^{3+} ions in alkali-metal borate glasses. *Phys. Rev. B Condens. Matter* **46**, 3305–3310, 10.1103/PhysRevB.46.3305 (1992).

50. Suresh Kumar, J. *et al.* Fluorescence characteristics of Dy^{3+} ions in calcium fluoroborate glasses. *J. Lumin.* **130**, 1916–1923, 10.1016/j.jlumin.2010.05.006 (2010).

51. Dwivedi, Y. & Rai, S. Spectroscopic study of Dy^{3+} and Dy^{3+}/Yb^{3+} ions co-doped in barium fluoroborate glass. *Opt. Mater. (Amst.)* **31**, 1472–1477, 10.1016/j.optmat.2009.02.005 (2009).

52. Jamalaiah, B. C. *et al.* Visible luminescence characteristics of Dy^{3+}-doped LBTAF glasses. *J. Alloy. Compd.* **474**, 382–387, 10.1016/j.jallcom.2008.06.094 (2009).

53. Pisarska, J. Optical properties of lead borate glasses containing Dy^{3+} ions. *J. Phys. Condens. Matter* **21**, 285101, 10.1088/0953-8984/21/28/285101 (2009).

54. Babu, P. & Jayasankar, C. K. Spectroscopic properties of Dy^{3+} ions in lithium borate and lithium fluoroborate glasses. *Opt. Mater. (Amst.)* **15**, 65–79, 10.1016/S0925-3467(00)00015-X (2000).

55. Ohishi, Y. *et al.* Pr^{3+}-doped fluoride fiber amplifier operating at 131 μm. *Opt. Lett.* **16**, 1747, 10.1364/OL.16.001747 (1991).

56. Saisudha, M. B. & Ramakrishna, J. Effect of host glass on the optical absorption properties of Nd^{3+}, Sm^{3+}, and Dy^{3+} in lead borate glasses. *Phys. Rev. B Condens. Matter* **53**, 6186–6196, 10.1103/PhysRevB.53.6186 (1996).

57. Adam, J. L. & Sibley, W. A. Optical transitions of Pr^{3+} ions in fluorozirconate glass. *J. Non Cryst. Solids* **76**, 267–279, 10.1016/0022-3093(85)90004-3 (1985).

58. Kumi-Barimah, E., Chen, Y., Sharma, G. & Jha, A. Judd-Ofelt analysis, visible to NIR photoluminescence emission under 450 nm and 976 nm excitations and energy transfer of barium fluorotellurite glasses doping with Ho^{3+}, Yb^{3+}, Ho^{3+}:Yb^{3+}. *Opt. Materials: X* **16**, 100201, 10.1016/j.omx.2022.100201 (2022).

59. Chen, R. *et al.* Efficient 2 μm emission in Nd^{3+} /Ho^{3+} co-doped silicate-germanate glass pumped by common 808 nm LD. *Opt. Laser Technol.* **89**, 108–113, 10.1016/j.optlastec.2016.09.036 (2017).

60. Hu, Z. *et al.* Spectroscopic investigations and Judd-Ofelt analysis of Sm^{3+} doped Y_2O_3 transparent ceramics. *Phys. B Condens. Matter* **669**, 415283, 10.1016/j.physb.2023.415283 (2023).

61. Li, W. *et al.* Crystal growth and visible fluorescence and energy transfer features of Dy^{3+}/RE^{3+} (RE = Tb, Eu)-codoped $Y_3Al_5O_{12}$ crystals. *J. Lumin.* **247**, 118864, 10.1016/j.jlumin.2022.118864 (2022).

62. Pan, Y. *et al.* Growth and optical properties of Dy:$Y_3Al_5O_{12}$ crystal. *Phys. B Condens. Matter* **530**, 317–321, 10.1016/j.physb.2017.12.001 (2018).

63. Brik, M. G., Ishii, T., Tkachuk, A. M., Ivanova, S. E. & Razumova, I. K. Calculations of the transitions intensities in the optical spectra of Dy^{3+}:$LiYF_4$. *J. Alloy. Compd.* **374**, 63–68, 10.1016/j.jallcom.2003.11.142 (2004).

64. Dominiak-Dzik, G., Ryba-Romanowski, W., Lisiecki, R., Solarz, P. & Berkowski, M. Dy-doped Lu_2SiO_5 single crystal: spectroscopic characteristics and luminescence dynamics. *Appl. Phys. B* **99**, 285–297, 10.1007/s00340-009-3852-x (2010).

65. Zhang, Y., Xu, J. & Lu, B. Spectroscopic properties of Dy^{3+}:$Bi_4Si_3O_{12}$ single crystal. *J. Alloy. Compd.* **582**, 635–639, 10.1016/j.jallcom.2013.08.090 (2014).

66. Sardar, D. K., Bradley, W. M., Yow, R. M., Gruber, J. B. & Zandi, B. Optical transitions and absorption intensities of Dy^{3+} ($4f^9$) in YSGG laser host. *J. Lumin.* **106**, 195–203, 10.1016/j.jlumin.2003.09.006 (2004).

67. Wang, Y., You, Z., Li, J., Zhu, Z. & Tu, C. Optical properties of Dy^{3+} ion in GGG laser crystal. *J. Phys. D Appl. Phys.* **43**, 075402, 10.1088/0022-3727/43/7/075402 (2010).

68. Lupei, A., Lupei, V., Gheorghe, C., Ikesue, A. & Enculescu, M. Spectroscopic characteristics of Dy^{3+} doped $Y_3Al_5O_{12}$ transparent ceramics. *J. Appl. Phys.* **110**, 083120, 10.1063/1.3656718 (2011).

69. Guo, H., Zhang, M., Han, J. & Nie, Y. Crystal growth, Judd–Ofelt analysis and radiative properties of Nd:YAG single crystal grown by HDS. *J. Lumin.* **140**, 135–137, 10.1016/j.jlumin.2013.03.002 (2013).

70. Strek, W., Bednarkiewicz, A., Hreniak, D., Mazur, P. & Lojkowski, W. Fabrication and optical properties of transparent Nd^{3+}:YAG nanoceramics. *J. Lumin.* **122-123**, 70–73, 10.1016/j.jlumin.2006.01.100 (2007).

71. Serqueira, E., Dantas, N., Monte, A. & Bell, M. Judd Ofelt calculation of quantum efficiencies and branching ratios of Nd^{3+} doped glasses. *J. Non Cryst. Solids* **352**, 3628–3632, https://doi.org/10.1016/j.jnoncrysol.2006.03.093 (2006).

72. Takebe, H., Murata, T., Nishida, H., Hewak, D. W. & Morinaga, K. Compositional dependence of optical properties of Nd^{3+} in gallate glasses. *J. Ceram. Soc. Jpn.* **104**, 243–246, 10.2109/jcersj.104.243 (1996).

73. Henrie, D. E. & Henrie, B. K. Hypersensitivity in the f-f transitions of hexabromo- and hexachlorneodymium(III). *J. Inorg. Nucl. Chem.* **39**, 1583–1586, 10.1016/0022-1902(77)80106-1 (1977).

74. Hanumanthu, M., Annapurna, K. & Buddhudu, S. Fluorescence characteristics of Nd^{3+} -doped heavy metal fluoride glasses. *Solid State Commun.* **80**, 315–320, 10.1016/0038-1098(91)90137-K (1991).

75. Weber, M. J., Saroyan, R. A. & Ropp, R. C. Optical properties of Nd^{3+} in metaphosphate glasses. *J. Non Cryst. Solids* **44**, 137–148, 10.1016/0022-3093(81)90138-1 (1981).

76. Alfrey, A. J., Stafsudd, O. M., Dunn, B. & Yang, D. L. Analysis of the absorption spectrum of neodymium:sodium beta double prime alumina. *J. Chem. Phys.* **88**, 707–716, 10.1063/1.454149 (1988).

77. Ratnakaram, Y. C. & Buddudu, S. Optical absorption spectra and laser analysis of Nd(III) in fluoroborate glasses. *Solid State Commun.* **97**, 651–655, 10.1016/0038-1098(95)00576-5 (1996).

78. Lomheim, T. S. & DeShazer, L. G. Optical-absorption intensities of trivalent neodymium in the uniaxial crystal yttrium orthovanadate. *J. Appl. Phys.* **49**, 5517–5522, 10.1063/1.324471 (1978).

79. Carnall, W. T., Fields, P. R. & Wybourne, B. G. Spectral intensities of the trivalent lanthanides and actinides in solution. I. Pr^{3+}, Nd^{3+}, Er^{3+}, Tm^{3+}, and Yb^{3+}. *J. Chem. Phys.* **42**, 3797–3806, 10.1063/1.1695840 (1965).

80. Henrie, D. E. & Smyser, C. E. Oscillator strengths of some lanthanide nitrates in tributylphosphate. *J. Inorg. Nucl. Chem.* **39**, 625–629, 10.1016/0022-1902(77)80576-9 (1977).

81. Sinha, S. P., Mehta, P. C. & Surana, S. Spectral intensities of lanthanide complexes. *Mol. Phys.* **23**, 807–813, 10.1080/00268977200100781 (1972).

82. Mehta, P. C. & Tandon, S. P. Spectral intensities of some Nd^{3+} β-diketonates. *J. Chem. Phys.* **53**, 414–417, 10.1063/1.1673796 (1970).

83. Oye, H. A. & Gruen, D. M. Neodymium chloride-aluminum chloride vapor complexes. *J. Am. Chem. Soc.* **91**, 2229–2236, 10.1021/ja01037a008 (1969).

84. Liu, C. S. & Zollweg, R. J. Complex molecules in cesium-rare earth iodide vapors. *J. Chem. Phys.* **60**, 2384–2390, 10.1063/1.1681373 (1974).

85. Bornstein, A. & Reisfeld, R. Laser emission cross-section and threshold power for laser operation at 1077 nm and 1370 nm; chalcogenide mini-lasers doped by Nd^{3+}. *J. Non Cryst. Solids* **50**, 23–27, 10.1016/0022-3093(82)90196-X (1982).

86. Reisfeld, R. Luminescence and prediction of transition probabilities for solar energy and lasers. *J. Less-common Met.* **112**, 9–18, 10.1016/0022-5088(85)90003-7 (1985).

87. Adam, J., Docq, A. & Lucas, J. Optical transitions of Dy^{3+} ions in fluorozirconate glass. *J. Solid State Chem.* **75**, 403–412, 10.1016/0022-4596(88)90181-8 (1988).

88. Greenberg, E. *et al.* Radiative transition probabilities of Er^{3+} in yttria stabilized cubic zirconia crystals. *J. Chem. Phys.* **77**, 4797–4803, 10.1063/1.443720 (1982).

89. Weber, M. J. Probabilities for radiative and nonradiative decay of Er^{3+} in LaF_3. *Phys. Rev.* **157**, 262–272, 10.1103/PhysRev.157.262 (1967).

90. Weber, M. J., Matsinger, B. H., Donlan, V. L. & Surratt, G. T. Optical transition probabilities for trivalent holmium in LaF_3 and $YAlO_3$. *J. Chem. Phys.* **57**, 562–567, 10.1063/1.1678000 (1972).

91. Shinn, M. D., Sibley, W. A., Drexhage, M. G. & Brown, R. N. Optical transitions of Er^{3+} ions in fluorozirconate glass. *Phys. Rev. B Condens. Matter* **27**, 6635–6648, 10.1103/PhysRevB.27.6635 (1983).

92. Xu, L.-W., Crosswhite, H. M. & Hessler, J. P. Fluorescent and dynamic properties of optically excited dysprosium trifluoride. *J. Chem. Phys.* **81**, 698–703, 10.1063/1.447752 (1984).

93. Tanimura, K., Shinn, M. D., Sibley, W. A., Drexhage, M. G. & Brown, R. N. Optical transitions of Ho^{3+} ions in fluorozirconate glass. *Phys. Rev. B Condens. Matter* **30**, 2429–2437, 10.1103/PhysRevB.30.2429 (1984).

94. Walsh, B. M. & Barnes, N. P. Comparison of Tm:ZBLAN and Tm:silica fiber lasers; spectroscopy and tunable pulsed laser operation around 1.9 μm. *Appl. Phys. B* **78**, 325–333, 10.1007/s00340-003-1393-2 (2004).

95. Ivanova, S. & Pellé, F. Strong 153 μm to NIR-VIS-UV upconversion in Er-doped fluoride glass for high-efficiency solar cells. *J. Opt. Soc. Am. B* **26**, 1930, 10.1364/JOSAB.26.001930 (2009).

96. Zhou, B., Pun, E. Y.-B., Lin, H., Yang, D. & Huang, L. Judd–Ofelt analysis, frequency upconversion, and infrared photoluminescence of Ho^{3+}-doped and Ho^{3+}/Yb^{3+}-codoped lead bismuth gallate oxide glasses. *J. Appl. Phys.* **106**, 103105, 10.1063/1.3256184 (2009).

97. Piatkowski, D. *et al.* Excited state absorption spectroscopy of ZBLAN:Ho^{3+} glass experiment and simulation. *J. Phys. Condens. Matter* **20**, 155201, 10.1088/0953-8984/20/15/155201 (2008).

98. Boyer, J. C., Vetrone, F., Capobianco, J. A., Speghini, A. & Bettinelli, M. Optical transitions and upconversion properties of Ho^{3+} doped $ZnOTeO_2$ glass. *J. Appl. Phys.* **93**, 9460–9465, 10.1063/1.1577817 (2003).

99. Sooraj Hussain, N. *et al.* Absorption and emission properties of Ho^{3+} doped lead-zinc-borate glasses. *Thin Solid Films* **515**, 318–325, 10.1016/j.tsf.2005.12.085 (2006).

100. Reddy, M. R., Raju, S. B. & Veeraiah, N. Optical absorption and fluorescence spectral studies of Ho^{3+} ions in $PbO–Al_2O_3–B_2O_3$ glass system. *J. Phys. Chem. Solids* **61**, 1567–1571, 10.1016/S0022-3697(00)00035-4 (2000).

101. Yuliantini, L. *et al.* Luminescence and Judd-Ofelt analysis of Nd^{3+} ion doped oxyfluoride boro-tellurite glass for near-infrared laser application. *Mater. Today* **43**, 2655–2662, 10.1016/j.matpr.2020.04.631 (2021).

102. Lalla, E. A. *et al.* Nd^{3+}-doped TeO_2–PbF_2–AlF_3 glasses for laser applications. *Opt. Mater. (Amst.)* **51**, 35–41, 10.1016/j.optmat.2015.11.010 (2016).

103. Mahraz, Z. A. S. *et al.* Spectroscopic investigations of near-infrared emission from Nd^{3+}-doped zinc-phosphate glasses: Judd-Ofelt evaluation. *J. Non Cryst. Solids* **509**, 106–114, 10.1016/j.jnoncrysol.2018.05.013 (2019).

104. Costa, F. B. *et al.* Spectroscopic properties of Nd^{3+}-doped tungsten–tellurite glasses. *J. Phys. Chem. Solids* **88**, 54–59, 10.1016/j.jpcs.2015.09.009 (2016).

105. Thomas, S. *et al.* Spectroscopic and dielectric studies of Sm^{3+} ions in lithium zinc borate glasses. *J. Non Cryst. Solids* **376**, 106–116, 10.1016/j.jnoncrysol.2013.05.022 (2013).

106. Jamalaiah, B. C., Suresh Kumar, J., Mohan Babu, A., Suhasini, T. & Rama Moorthy, L. Photoluminescence properties of Sm^{3+} in LBTAF glasses. *J. Lumin.* **129**, 363–369, 10.1016/j.jlumin.2008.11.001 (2009).

107. Wachtler, M. *et al.* Optical properties of rare-earth ions in lead germanate glasses. *J. Am. Ceram. Soc.* **81**, 2045–2052, 10.1111/j.1151-2916.1998.tb02586.x (2005).

108. Balda, R., Lacha, L. M., Fernández, J. & Fernández-Navarro, J. M. Optical spectroscopy of Tm^{3+} ions in GeO_2–PbO–Nb_2O_5 glasses. *Opt. Mater. (Amst.)* **27**, 1771–1775, 10.1016/j.optmat.2004.11.048 (2005).

109. Takebe, H., Nageno, Y. & Morinaga, K. Compositional dependence of Judd-ofelt parameters in silicate, borate, and phosphate glasses. *J. Am. Ceram. Soc.* **78**, 1161–1168, 10.1111/j.1151-2916.1995.tb08463.x (1995).

110. Wang, B. *et al.* Excited state absorption cross sections of $^4i_{13/2}$ of Er^{3+} in ZBLAN. *Opt. Mater. (Amst.)* **31**, 1658–1662, 10.1016/j.optmat.2009.03.015 (2009).

111. Takebe, H. *et al.* Spectroscopic properties of Nd^{3+} and Pr^{3+} in gallate glasses with low phonon energies. *Appl. Opt.* **36**, 5839, 10.1364/AO.36.005839 (1997).

112. Vařák, P., Nekvindová, P., Baborák, J. & Oswald, J. Near-infrared photoluminescence properties of Er/Yb- and Ho/Yb-doped multicomponent silicate glass – the role of GeO_2, Al_2O_3 and ZnO. *J. Non Cryst. Solids* **582**, 121457, 10.1016/j.jnoncrysol.2022.121457 (2022).

113. Lalla, E. A. *et al.* Judd-Ofelt parameters of RE^{3+}-doped fluorotellurite glass (RE^{3+}= Pr^{3+}, Nd^{3+}, Sm^{3+}, Tb^{3+}, Dy^{3+}, Ho^{3+}, Er^{3+}, and Tm^{3+}). *J. Alloy. Compd.* **845**, 156028, 10.1016/j.jallcom.2020.156028 (2020).

114. Uhlmann, E. V. *et al.* Spectroscopic properties of rare-earth-doped calcium-aluminate-based glasses. *J. Non Cryst. Solids* **178**, 15–22, 10.1016/0022-3093(94)90259-3 (1994).

115. Sardar, D. K. *et al.* Spectroscopic analysis and the effects of color centers on the laser performance of Nd^{3+}: $CaZn_2Y_2Ge_3O_{12}$. *Opt. Mater. (Amst.)* **3**, 257–263, 10.1016/0925-3467(94)90038-8 (1994).

116. Krupke, W. Radiative transition probabilities within the $4f^3$ground configuration of Nd:YAG. *IEEE J. Quantum Electron.* **7**, 153–159, https://doi.org/10.1109/JQE.1971.1076623 (1971).

117. Pecoraro, E., Sampaio, J. A., Nunes, L. A. O., Gama, S. & Baesso, M. L. Spectroscopic properties of water free Nd_2O_3-doped low silica calcium aluminosilicate glasses. *J. Non Cryst. Solids* **277**, 73–81, 10.1016/S0022-3093(00)00316-1 (2000).

118. Li, B., Feng, G., Gao, X., Yang, H. & Yang, C. Temperature and concentration dependence of spectroscopic properties of Nd^{3+}-doped yttrium aluminum garnet crystal. *Phys. B Condens. Matter* **407**, 3499–3503, 10.1016/j.physb.2012.05.009 (2012).

119. Kumar, G. A. *et al.* Spectroscopic and stimulated emission characteristics of Nd^{3+} in transparent YAG ceramics. *IEEE J. Quantum Electron.* **40**, 747–758, 10.1109/JQE.2004.828263 (2004).

120. Sardar, D. K., Yow, R. M., Gruber, J. B., Allik, T. H. & Zandi, B. Stark components of lower-lying manifolds and emission cross-sections of intermanifold and inter-stark transitions of $Nd^{3+}(4f^3)$ in polycrystalline ceramic garnet $Y_3Al_5O_{12}$. *J. Lumin.* **116**, 145–150, 10.1016/j.jlumin.2005.08.003 (2006).

121. Hou, X., Zhou, S., Jia, T., Lin, H. & Teng, H. Effect of Nd concentration on structural and optical properties of Nd:Y_2O_3 transparent ceramic. *J. Lumin.* **131**, 1953–1958, 10.1016/j.jlumin.2011.03.059 (2011).

122. Sato, Y., Taira, T. & Ikesue, A. Spectral parameters of nd3+-ion in the polycrystalline solid-solution composed of $Y_3Al_5O_{12}$ and $Y_3Sc_2Al_3O_{12}$. *Jpn. J. Appl. Phys. (2008)* **42**, 5071–5074, 10.1143/JJAP.42.5071 (2003).

123. Kumar, V. R. K., Bhatnagar, A. K. & Jagannathan, R. Structural and optical studies of Pr^{3+}, Nd^{3+}, Er^{3+} and Eu^{3+} ions in tellurite based oxyfluoride, TeO_2-LiF, glass. *J. Phys. D Appl. Phys.* **34**, 1563–1568, 10.1088/0022-3727/34/11/301 (2001).

124. Dulick, M., Faulkner, G. E., Cockroft, N. J. & Nguyen, D. C. Spectroscopy and dynamics of upconversion in Tm^{3+}: $YLiF_4$. *J. Lumin.* **48-49**, 517–521, 10.1016/0022-2313(91)90183-V (1991).

125. Reisfeld, R. & Eckstein, Y. Dependence of spontaneous emission and nonradiative relaxations of Tm^{3+} and Er^{3+} on glass host and temperature. *J. Chem. Phys.* **63**, 4001–4012, 10.1063/1.431839 (1975).

126. Leavitt, R. P. & Morrison, C. A. Crystal-field analysis of triply ionized rare earth ions in lanthanum trifluoride. II. intensity calculations. *J. Chem. Phys.* **73**, 749–757, 10.1063/1.440180 (1980).

127. Krupke, W. F. & Gruber, J. B. Optical-absorption intensities of rare-earth ions in crystals: The absorption spectrum of thulium ethyl sulfate. *Phys. Rev.* **139**, A2008–A2016, 10.1103/PhysRev.139.A2008 (1965).

128. Carnall, W. T., Beitz, J. V., Crosswhite, H., Rajnak, K. & Mann, J. B. *Spectroscopic properties of the f-elements in compounds and solutions. [79 references]* (Office of Scientific and Technical Information (OSTI), 1982).

129. Weber, M. J., Varitimos, T. E. & Matsinger, B. H. Optical intensities of rare-earth ions in yttrium orthoaluminate. *Phys. Rev.* **8**, 47–53, 10.1103/PhysRevB.8.47 (1973).

130. Yeh, D. C., Sibley, W. A. & Suscavage, M. J. Efficient frequency upconversion of Tm^{3+} ions in Yb^{3+} doped barium-thorium fluoride glass. *J. Appl. Phys.* **63**, 4644–4650, 10.1063/1.340117 (1988).

131. Özen, G. *et al.* Optical properties and upconverted emissions of Tm^{3+} in Yb^{3+} doped fluorophosphate glasses. *J. Phys. Chem. Solids* **54**, 1533–1542, 10.1016/0022-3697(93)90347-T (1993).

132. Özen, G. *et al.* Excited state absorption mechanisms of red to UV and blue conversion luminescence in Tm^{3+} doped fluorophosphate glass. *J. Lumin.* **63**, 85–96, 10.1016/0022-2313(94)00043-C (1995).

133. Peacock, R. D. Spectral intensities of the trivalent lanthanides. *Mol. Phys.* **25**, 817–823, 10.1080/00268977300100711 (1973).

134. Eyal, M., Reisfield, R., Schiller, A., Jacobani, C. & Jørgensen, C. K. Energy transfer between manganese(II) and thulium(III) in transition-metal fluoride glasses. *Chem. Phys. Lett.* **140**, 595–602, 10.1016/0009-2614(87)80494-3 (1987).

135. Tanabe, S., Hanada, T., Ohyagi, T. & Soga, N. Correlationbetween Eu^{151}Mössbauer isomer shift and Judd-Ofelt Ω_6 parameters of Nd^{3+} ions in phosphate and silicate laser glasses. *Phys. Rev. B Condens. Matter* **48**, 10591–10594, 10.1103/PhysRevB.48.10591 (1993).

136. Tanabe, S., Tamai, K., Hirao, K. & Soga, N. Branching ratio of uv and blue upconversions of Tm^{3+} ions in glasses. *Phys. Rev. B Condens. Matter* **53**, 8358–8362, 10.1103/PhysRevB.53.8358 (1996).

137. Joubert, M. F., Guy, S., Linarès, C., Jacquier, B. & Adam, J. L. Avalanche upconversion in Tm^{3+}-doped BIGaZYTZr glass. *J. Non Cryst. Solids* **184**, 98–102, 10.1016/0022-3093(95)00090-9 (1995).

138. Peng, B. & Izumitani, T. Optical properties, fluorescence mechanisms and energy transfer in Tm^{3+}, Ho^{3+} and Tm^{3+} -Ho^{3+} doped near-infrared laser glasses, sensitized by Yb^{3+}. *Opt. Mater. (Amst.)* **4**, 797–810, 10.1016/0925-3467(95)00032-1 (1995).

139. Hirao, K., Tamai, K., Tanabe, S. & Soga, N. Frequency upconversion and its new mechanism in Tm^{3+}-doped fluoroaluminate glasses. *J. Non Cryst. Solids* **160**, 261–267, 10.1016/0022-3093(93)91270-D (1993).

140. Yeh, D. C. *et al.* Energy transfer between Er^{3+} and Tm^{3+} ions in a barium fluoride-thorium fluoride glass. *Phys. Rev. B Condens. Matter* **39**, 80–90, 10.1103/PhysRevB.39.80 (1989).

141. Li, C. *et al.* Luminescence properties of the Tm^{3+} doped silicates Y_2SiO_5, $CaY_4(SiO_4)_3O$ and $SrY_4(SiO_4)_3O$. *J. Lumin.* **62**, 157–171, 10.1016/0022-2313(94)90342-5 (1994).

142. Guery, C., Adam, J. L. & Lucas, J. Optical properties of Tm^{3+} ions in indium-based fluoride glasses. *J. Lumin.* **42**, 181–189, 10.1016/0022-2313(88)90037-3 (1988).

143. Oomen, E. W. J. L. Up-conversion of red light into blue light in thulium doped fluorozirconate glasses. *J. Lumin.* **50**, 317–332, 10.1016/0022-2313(92)90081-J (1992).

144. Villacampa, B. *et al.* Optical properties of ZnF_2-CdF_2 glasses doped with 4f ions. *Mater. Res. Bull.* **26**, 741–748, 10.1016/0025-5408(91)90063-R (1991).

145. Heo, J., Shin, Y. B. & Jang, J. N. Spectroscopic analysis of Tm^{3+} in PbO-Bi_2O_3-Ga_2O_3 glass. *Appl. Opt.* **34**, 4284, 10.1364/AO.34.004284 (1995).

146. Tanabe, S. & Hanada, T. Effect of ligand field on branching ratio of ultraviolet and blue upconversions of Tm^{3+} ions in halide and oxide glasses. *J. Appl. Phys.* **76**, 3730–3734, 10.1063/1.357444 (1994).

147. Kermaoui, A., Barthou, C., Denis, J.-P. & Blanzat, B. Spectroscopic properties of Tm^{3+} in fluorophosphate glasses. *J. Lumin.* **29**, 295–308, 10.1016/0022-2313(84)90028-0 (1984).

148. Krupke, W. F. Optical absorption and fluorescence intensities in several rare-earth-DopedY_2O_3 and LaF_3 Single crystals. *Phys. Rev.* **145**, 325–337, 10.1103/PhysRev.145.325 (1966).

149. Wetenkamp, L., West, G. F. & Többen, H. Optical properties of rare earth-doped ZBLAN glasses. *J. Non Cryst. Solids* **140**, 35–40, 10.1016/S0022-3093(05)80737-9 (1992).

150. Razumova, I., Tkachuk, A., Nikitichev, A. & Mironov, D. Spectral-luminescent properties of Tm:YLF crystal. *J. Alloy. Compd.* **225**, 129–132, https://doi.org/10.1016/0925-8388(94)07022-9 (1995).

151. Sanz, J., Cases, R. & Alcalá, R. Optical properties of Tm^{3+} in fluorozirconate glass. *J. Non Cryst. Solids* **93**, 377–386, 10.1016/S0022-3093(87)80182-5 (1987).

152. Villacampa, B. *et al.* Optical properties of 4f-ions in ZnF_2-CdF_2 doped glasses. *Mater. Sci. For.* **67-68**, 527–532, 10.4028/www.scientific.net/MSF.67-68.527 (1991).

153. Cases, R. & Chamarro, M. A. Judd-Ofelt analysis and multiphonon relaxations of rare earth ions in fluorohafnate glasses. *J. Solid State Chem.* **90**, 313–319, 10.1016/0022-4596(91)90148-B (1991).

154. Tanabe, S., Suzuki, K., Soga, N. & Hanada, T. Selective sensitization of 480-nm blue upconversion by Tm^{3+}-Er^{3+} energy transfer in tellurite glass. *J. Opt. Soc. Am. B* **11**, 933, 10.1364/JOSAB.11.000933 (1994).

155. Seeber, W., Arnold, P. & Ehrt, D. Luminescence properties and energy transfer in Ce^{3+} and/or Tm^{3+} doped fluoride phosphate glasses. *Phys. Status Solidi A Appl. Res.* **130**, K243–K246, 10.1002/pssa.2211300255 (1992).

156. Bukietynska, K. & Choppin, G. R. Environmental effects on f–f transitions. III. spectral intensities of lanthanide nitrate, sulfate, and α-picolinate solutions. *J. Chem. Phys.* **52**, 2875–2880, 10.1063/1.1673415 (1970).

157. Núñez, L. *et al.* Optical absorption and luminescence of Tm^{3+}-doped $LiNbO_3$ and $LiNbO_3$ (MgO) crystals. *J. Lumin.* **55**, 253–263, 10.1016/0022-2313(93)90020-N (1993).

158. Reddy, A. V. R., Balaji, T. & Buddhudu, S. Absorption and photoluminescence spectra of Tm^{3+}-doped fluorophosphate glasses. *Spectrochim. Acta A* **48**, 1515–1521, 10.1016/0584-8539(92)80162-P (1992).

159. Spector, N., Reisfeld, R. & Boehm, L. Eigenstates and radiative transition probabilities for Tm^{3+} ($4f^{12}$) in phosphate and tellurite glasses. *Chem. Phys. Lett.* **49**, 49–53, 10.1016/0009-2614(77)80439-9 (1977).

160. Carnall, W. T., Hessler, J. P. & Wagner, F. W., Jr. Transition probabilities in the absorption and fluorescence spectra of lanthanides in molten lithium nitrate -potassium nitrate eutectic. *J. Phys. Chem.* **82**, 2152–2158, 10.1021/j100509a003 (1978).

161. Rukmini, E. & Jayasankar, C. K. Optical properties of Tm^{3+} ions in zinc borosulphate glasses and comparative energy level analyses of Tm^{3+} ions in various glasses. *J. Non Cryst. Solids* **176**, 213–229, 10.1016/0022-3093(94)90080-9 (1994).

162. Wang, Q. Y., Zhang, S. Y. & Jia, Y. Q. Effect of the concentration of the Er^{3+} ion on the spectral intensity parameters of Er:YAG crystals. *J. Alloy. Compd.* **202**, 1–5, 10.1016/0925-8388(93)90507-J (1993).

163. Hubert, S., Meichenin, D., Zhou, B. W. & Auzel, F. Emission properties, oscillator strengths and laser parameters of Er^{3+} in $LiYF_4$ at 2.7 μm. *J. Lumin.* **50**, 7–15, 10.1016/0022-2313(91)90004-F (1991).

164. Ledig, M., Heumann, E., Ehrt, D. & Seeber, W. Spectroscopic and laser properties of Cr^{3+}:Yb^{3+}:Er^{3+}: fluoride phosphate glass. *Opt. Quantum Electron.* **22**, S107–S122, 10.1007/BF02089004 (1990).

165. Naidu, K. S. & Buddhudu, S. Photoluminescence properties of Er^{3+}-doped $(NaPO_3)_6$-$BaCl_2$-$ZnCl_2$-RCl glasses. *Mater. Lett.* **13**, 299–305, 10.1016/0167-577X(92)90056-P (1992).

166. Merino, R. I., Orera, V. M., Cases, R. & Chamarro, M. A. Spectroscopic characterization of Er^{3+} in stabilized zirconia single crystals. *J. Phys. Condens. Matter* **3**, 8491–8502, 10.1088/0953-8984/3/43/015 (1991).

167. Kaminskii, A. A. *et al.* Spectroscopic properties and 3 μm stimulated emission of Er^{3+} ions in the $(Y_{1x}Er_x)_3Al_5O_{12}$ and $(Lu_{1x}Er_3)_3Al_5O_{12}$ garnet crystal systems. *Phys. Status Solidi A Appl. Res.* **71**, 291–312, 10.1002/pssa.2210710202 (1982).

168. Kaminskii, A. A., Mironov, V. S. & Bagaev, S. N. New laser potentialities of insulating generating crystals doped with Er^{3+} ions. *Phys. Status Solidi A Appl. Res.* **148**, K107–K110, 10.1002/pssa.2211480245 (1995).

169. Chen, C. Y., Sibley, W. A., Yeh, D. C. & Hunt, C. A. The optical properties of Er^{3+} and Tm^{3+} in $KCaF_3$ crystal. *J. Lumin.* **43**, 185–194, 10.1016/0022-2313(89)90001-X (1989).

170. Renuka Devi, A. & Jayasankar, C. K. Optical properties of Er^{3+} ions in lithium borate glasses and comparative energy level analyses of Er^{3+} ions in various glasses. *J. Non Cryst. Solids* **197**, 111–128, 10.1016/0022-3093(95)00573-0 (1996).

171. Kaminskii, A. A., Butashin, A. V., Mironov, V. S., Bagaev, S. N. & Eichler, H.-J. Efficient 2 μm stimulated emission in the $^4F_{9/2} \rightarrow {}^4I_{11/2}$ channel from monoclinic $BaYb_2F_8$: Er^{3+} crystals. *Phys. Status Solidi B Basic Res.* **194**, 319–332, 10.1002/pssb.2221940128 (1996).

172. Yanagita, H., Okada, K., Miura, K., Toratani, H. & Yamashita, T. Er^{3+} doped fluorozirco-aluminate glasses. *Mater. Sci. For.* **67-68**, 521–526, 10.4028/www.scientific.net/MSF.67-68.521 (1991).

173. Kaminskii, A. A. *et al.* Growth, spectroscopy, and stimulated emission of cubic $Bi_4Ge_3O_{12}$ crystals doped with Dy^{3+}, Ho^{3+}, Er^{3+}, Tm^{3+}, or Yb^{3+} ions. *Phys. Status Solidi A Appl. Res.* **56**, 725–736, 10.1002/pssa.2210560240 (1979).

174. Ryba-Romanowski, W., Mazurak, Z., Jeżowska-trzebiatowska, B., Schultze, D. & Waligora, C. Growth and spectroscopic properties of $LiErP_4O_{12}$ single crystals. *Phys. Status Solidi A Appl. Res.* **62**, 75–81, 10.1002/pssa.2210620107 (1980).

175. Tanabe, S., Takahara, K., Takahashi, M. & Kawamoto, Y. Spectroscopic studies of radiative transitions and upconversion characteristics of Er^{3+} ions in simple pseudoternary fluoride glasses MF_n–BaF_2–YF_3 (M: Zr, Hf, Al, Sc, Ga, In, or Zn). *J. Opt. Soc. Am. B* **12**, 786, 10.1364/JOSAB.12.000786 (1995).

176. Adam, J. L., Matecki, M. & Lucas, J. Multiphonon relaxations in chloro-fluoride glasses. *J. Non Cryst. Solids* **184**, 119–123, 10.1016/0022-3093(94)00604-0 (1995).

177. Keller, B., Bukietyńska, K. & Jeżowska-Trzebiatowska, B. Intensity of f-f bands of heavy lanthanide chloride alcohol solvates. *Chem. Phys. Lett.* **92**, 541–547, 10.1016/0009-2614(82)87056-5 (1982).

178. Zou, X. & Izumitani, T. Spectroscopic properties and mechanisms of excited state absorption and energy transfer upconversion for Er^{3+}-doped glasses. *J. Non Cryst. Solids* **162**, 68–80, 10.1016/0022-3093(93)90742-G (1993).

179. Eyal, M., Reisfeld, R., Jørgensen, C. K. & Bendow, B. Laser properties of holmium and erbium in thorium-, zinc- and yttrium-based fluoride glass. *Chem. Phys. Lett.* **139**, 395–400, 10.1016/0009-2614(87)80580-8 (1987).

180. Legendziewicz, J., Oczko, G. & Meyer, G. Spectroscopy studies of lanthanide trichloroacetate single crystals. *Polyhedron* **10**, 1921–1928, 10.1016/S0277-5387(00)86056-8 (1991).

181. Kanoun, A., Alaya, S. & Maaref, H. Spectroscopic properties of Pr^{3+} and Nd^{3+} ions in zinc tellurite glasses. *Phys. Status Solidi B Basic Res.* **162**, 523–529, 10.1080/07315179208203353 (1990).

182. Reddy, A. V. R. *et al.* Photoluminescence spectra of Er^{3+}-doped fluorophosphate glasses. *Ferroelectr. Lett.* **14**, 145–159, 10.12693/APhysPolA.90.233 (1992).

183. Mondry, A. & Bukietyńska, K. Spectroscopy studies of erbium and dysprosium acetate single crystals. *Acta Phys. Pol. A.* **90**, 233–238, 10.1016/0925-8388(95)01613-9 (1996).

184. Florez, A., Messaddeq, Y., Malta, O. L. & Aegerter, M. A. Optical transition probabilities and compositional dependence of Judd-Ofelt parameters of Er^{3+} ions in fluoroindate glass. *J. Alloy. Compd.* **227**, 135–140, 10.1109/3.135248 (1995).

185. Li, C., Wyon, C. & Moncorge, R. Spectroscopic properties and fluorescence dynamics of Er^{3+} and Yb^{3+} in Y_2SiO_5. *IEEE J. Quantum Electron.* **28**, 1209–1221, 10.1016/0022-4596(82)90143-8 (1992).

186. Reisfeld, R. *et al.* Optical transition probabilities of Er^{3+} in fluoride glasses. *J. Solid State Chem.* **41**, 253–261, 10.1016/0022-2313(94)90062-0 (1982).

187. Souriau, J. C., Borel, C., Wyon, C., Li, C. & Moncorgé, R. Spectroscopic properties and fluorescence dynamics of Er^{3+} and Yb^{3+} in $CaYAlO_4$. *J. Lumin.* **59**, 349–359, 10.1016/S0020-1693(00)90447-X (1994).

188. Bukietynska, K. & Mondry, A. Spectroscopy of heavy lanthanide complexes with NTA. *Inorganica Chim. Acta* **130**, 271–276, 10.1002/pssa.2211550125 (1987).

189. Simondi-Teisseire, B., Viana, B., Vivien, D. & Lejus, A. M. Optical investigation of Er:$Ca_2Al_2SiO_7$ and Yb:$Ca_2Al_2SiO_7$ for laser applications in the near infrared. *Phys. Status Solidi A Appl. Res.* **155**, 249–262, 10.1063/1.362621 (1996).

190. Pan, Z., Morgan, S. H., Dyer, K., Ueda, A. & Liu, H. Host-dependent optical transitions of Er^{3+} ions in lead–germanate and lead-tellurium-germanate glasses. *J. Appl. Phys.* **79**, 8906–8913, 10.1021/ic00255a006 (1996).

191. Devlin, M. T., Stephens, E. M., Richardson, F. S., Van Cott, T. C. & Davis, S. A. Empirical intensity parameters for the 4f−4f absorption spectra of nine-coordinate erbium(III) complexes in aqueous solution. *Inorg. Chem.* **26**, 1204–1207, 10.1016/0022-2313(90)90036-B (1987).

192. Ryba-Romanowski, W. Effect of temperature and activator concentration on luminescence decay of erbium-doped tellurite glass. *J. Lumin.* **46**, 163–172, 10.2109/jcersj.101.78 (1990).

193. Tanabe, S., Ohyagi, T., Hanada, T. & Soga, N. Upconversion and local structure of Er^{3+} doped aluminate glasses. *J. Ceram. Soc. Jpn.* **101**, 78–83, 10.1016/0022-2313(96)00063-4 (1993).

194. Amin, J., Dussardier, B., Schweizer, T. & Hempstead, M. Spectroscopic analysis of Er^{3+} transitions in lithium niobate. *J. Lumin.* **69**, 17–26, 10.1016/0030-4018(92)90306-C (1996).

195. Huang, Y., Luo, Z. & Wang, G. Optical transition probabilities for Er^{3+} in KY $(WO_4)_2$ crystal. *Opt. Commun.* **88**, 42–46, 10.1002/pssa.2211200123 (1992).

196. Kaminskii, A. A., Mill, B. V., Butashin, A. V., Kurbanov, K. & Polyakova, L. A. Spectroscopy of disordered $La_3Ga_5SiO_{14}$ single crystals doped with Pr^{3+}, Ho^{3+}, and Er^{3+} ions. *Phys. Status Solidi A Appl. Res.* **120**, 253–266, 10.1016/S0020-1693(00)80373-4 (1990).

197. Ingletto, G., Bettinelli, M., Di Sipio, L., Negrisolo, F. & Aschieri, C. Optical transition intensities of trivalent lanthanide ions in zinc and lead metaphosphate glasses. *Inorganica Chim. Acta* **188**, 201–204, 10.1016/0167-577X(90)90061-P (1991).

198. Subramanyam, Y., Moorthy, L. R. & Lakshman, S. V. J. Spectral intensities and Judd-Ofelt parameterization of er-doped ternary sulphate glasses. *Mater. Lett.* **9**, 277–283, 10.1002/pssb.2221950132 (1990).

199. Kumar, V. V. R. K., Jayasankar, C. K. & Jagannathan, R. Optical properties of Er^{3+} ions in zinc borosulphate glasses. *Phys. Status Solidi B Basic Res.* **195**, 287–296, 10.1021/ic50226a038 (1996).

200. Kirby, A. F. & Palmer, R. A. Hypersensitive transition probability in tris(1,3-diphenyl-1,3-propanedionato)aquolanthanides(III). *Inorg. Chem.* **20**, 4219–4222, 10.1021/ba-1967-0071.ch008 (1981).

201. Gruen, D. M., Dekock, C. W. & Mcbeth, R. L. *Electronic spectra of lanthanide compounds in the vapor phase*. Advances in chemistry series (AMERICAN CHEMICAL SOCIETY, WASHINGTON, D.C., 1967).

202. Alonso, P. J., Orera, V. M., Cases, R., Alcalá, R. & Rodríguez, V. D. Optical properties of Gd^{3+} in fluorozirconate glasses. *J. Lumin.* **39**, 275–282, 10.1016/S0009-2614(97)01126-3 (1988).

203. Binnemans, K., Görller-Walrand, C. & Adam, J. L. Spectroscopic properties of Gd^{3+}-doped fluorozirconate glass. *Chem. Phys. Lett.* **280**, 333–338, 10.1016/0022-3093(90)90226-C (1997).

204. Amaranath, G., Buddhudu, S. & Bryant, F. J. Spectroscopic properties of Tb^{3+}-doped fluoride glasses. *J. Non Cryst. Solids* **122**, 66–73, 10.1016/0022-3697(89)90061-9 (1990).

205. Verwey, J. W. M., Imbusch, G. F. & Blasse, G. Laser excited spectroscopy of Gd^{3+} ions in crystalline and glass borate hosts with comparable composition. *J. Phys. Chem. Solids* **50**, 813–820, 10.1063/1.441517 (1989).

206. Caird, J. A., Carnall, W. T. & Hessler, J. P. The terbium chloride–aluminum chloride vapor system. III. spectral intensity analysis. *J. Chem. Phys.* **74**, 3225–3233, 10.1016/0925-3467(95)00064-X (1981).

207. Duhamel-Henry, N., Adam, J. L., Jacquier, B. & Linarès, C. Photoluminescence of new fluorophosphate glasses containing a high concentration of terbium (III) ions. *Opt. Mater. (Amst.)* **5**, 197–207, 10.1016/0022-2313(95)00073-9 (1996).

208. Dejneka, M., Snitzer, E. & Riman, R. E. Blue, green and red fluorescence and energy transfer of Eu^{3+} in fluoride glasses. *J. Lumin.* **65**, 227–245, 10.1016/0022-4596(80)90566-6 (1995).

209. Blanzat, B., Boehm, L., Jørgensen, C. K., Reisfeld, R. & Spector, N. Transition probabilities of europium(III) in zirconium and beryllium fluoride glasses, phosphate glass, and pentaphosphate crystals. *J. Solid State Chem.* **32**, 185–192, 10.1016/0038-1098(90)90728-T (1980).

210. Harinath, R., Buddhudu, S., Bryant, F. J. & Xi, L. Absorption and fluorescence properties of Eu^{3+} doped alkali mixed heavy metal fluoride glasses. *Solid State Commun.* **74**, 1147–1152, 10.1063/1.436279 (1990).

211. Porcher, P. & Caro, P. Crystal field parameters for Eu^{3+} in KY3F1. II. intensity parameters. *J. Chem. Phys.* **68**, 4176–4182, 10.1016/0584-8539(93)80262-9 (1978).

212. Annapurna, K. & Buddhudu, S. Fluorescence of Eu^{3+}-doped InF_3-based optical glasses. *Spectrochim. Acta A* **49**, 73–80, 10.1016/S0022-3093(96)00406-1 (1993).

213. Binnemans, K. *et al.* Optical absorption and magnetic circular dichroism spectra of neodymium doped fluorozirconate (ZBLAN) glass. *J. Non Cryst. Solids* **204**, 178–187, 10.1016/0022-3093(94)90324-7 (1996).

214. Nageno, Y., Takebe, H., Morinaga, K. & Izumitani, T. Effect of modifier ions on fluorescence and absorption of Eu^{3+} in alkali and alkaline earth silicate glasses. *J. Non Cryst. Solids* **169**, 288–294, https://doi.org/10.1016/S0009-2614(97)00012-2 (1994).

215. Binnemans, K., Van Herck, K. & Görller-Walrand, C. Influence of dipicolinate ligands on the spectroscopic properties of europium(III) in solution. *Chem. Phys. Lett.* **266**, 297–302, 10.1103/PhysRevB.54.12076 (1997).

216. Balda, R., Fernández, J., Adam, J. L. & Arriandiaga, M. A. Time-resolved fluorescence-line narrowing and energy-transfer studies in a Eu^{3+}-doped fluorophosphate glass. *Phys. Rev. B Condens. Matter* **54**, 12076–12086, 10.1016/0925-8388(94)90263-1 (1996).

217. de Sá, G. F., e Silva, F. R. G. & Malta, O. L. Synthesis, spectroscopy and photophysical properties of mixed ligand complexes of europium(III) and terbium(III). *J. Alloy. Compd.* **207-208**, 457–460, 10.1007/BF02841439 (1994).

218. Nachimuthu, P. & Jagannathan, R. Absorption and emission spectral studies of Eu^{3+}-doped PbO-PbF_2 glass system. *J. Chem. Sci. (Bangalore)* **107**, 59–66, 10.1021/ic50226a038 (1995).

219. Kirby, A. F. & Palmer, R. A. Hypersensitive transition probability in tris(1,3-diphenyl-1,3-propanedionato)aquolanthanides(III). *Inorg. Chem.* **20**, 4219–4222, 10.1080/00319109108030635 (1981).

220. Buddhudu, S., Rangarajan, V. N., Amaranath, G., Harinath, R. & Kumar, A. S. Optical properties of $Ho(NO_3)_3 6H_2O$: Organic acid complexes. *Phys. Chem. Liq.* **23**, 61–68, 10.1016/0022-4596(79)90060-4 (1991).

221. Boehm, L., Reisfeld, R. & Spector, N. Optical transitions of Sm^{3+} in oxide glasses. *J. Solid State Chem.* **28**, 75–78, 10.1016/0167-577X(92)90053-M (1979).

222. Naidu, K. S. & Buddhudu, S. Photoluminescence properties of Ho^{3+}-doped $(NaPO_3)_6$-$BaCl_2$-$ZnCl_2$-RCl glasses. *Mater. Lett.* **14**, 355–360, 10.1016/S0020-1693(00)83131-X (1992).

223. Mondry, A. Spectroscopic properties of Ho^{3+} complexes with dipicolinic acid in solufion and single crystals. *Inorganica Chim. Acta* **162**, 131–137, 10.1016/0584-8539(88)80186-7 (1989).

224. Buddhudu, S. & Bryant, F. J. Optical properties of Ho^{3+}: Alkali mixed fluoride glasses. *Spectrochim. Acta A* **44**, 1381–1385, 10.1080/07315179308205931 (1988).

225. Ranga Reddy, A. V., Annapurna, K., Jacob, A. S. & Buddhudu, S. Fluorescence properties of Ho^{3+} doped fluorophosphate glasses. *Ferroelectr. Lett.* **15**, 33–44, 10.1063/1.432659 (1993).

226. Reisfeld, R. & Hormadaly, J. Optical intensities of holmium in tellurite, calibo, and phosphate glasses. *J. Chem. Phys.* **64**, 3207–3212, 10.1007/BF00563573 (1976).

227. Shin, Y. B., Jang, J. N. & Heo, J. Mid-infrared light emission characteristics of Ho^{3+}-doped chalcogenide and heavy-metal oxide glasses. *Opt. Quantum Electron.* **27**, 379–386, 10.1016/0022-2313(85)90109-7 (1995).

228. Adam, J. L., Sibley, W. A. & Gabbe, D. R. Optical absorption and emission of $LiYF_4$:Ho^{3+}. *J. Lumin.* **33**, 391–407, 10.1002/pssb.2221620224 (1985).

229. Heo, J. & Shin, Y. B. Absorption and mid-infrared emission spectroscopy of Dy^{3+} in Ge-As(or Ga)-S glasses. *J. Non Cryst. Solids* **196**, 162–167, 10.1016/0022-3093(95)00579-X (1996).

230. Hewak, D. W., Payne, D. N., Medeiros Neto, J. A., Laming, R. I. & Samson, B. N. Emission at 1.3 μm from dysprosium-doped Ga:La:S glass. *Electron. Lett.* **30**, 968–970, 10.1049/el:19940645 (1994).

231. Wei, K., Machewirth, D. P., Wenzel, J., Snitzer, E. & Sigel, G. H. Spectroscopy of Dy^{3+} in Ge–Ga–S glass and its suitability for 13-μm fiber-optical amplifier applications. *Opt. Lett.* **19**, 904, 10.1364/OL.19.000904 (1994).

232. Malinowski, M. *et al.* Spectroscopic and laser properties of $LiNbO_3$:Dy^{3+}crystals. *Acta Phys. Pol. A.* **90**, 181–189, 10.12693/APhysPolA.90.181 (1996).

233. Eyal, M., Greenberg, E., Reisfeld, R. & Spector, N. Spectroscopy of praseodymium(III) in zirconium fluoride glass. *Chem. Phys. Lett.* **117**, 108–114, 10.1016/0009-2614(85)85216-7 (1985).

234. Malinowski, M., Wolski, R. & Woliński, W. Absorption intensity analysis of Pr^{3+}: $Y_3Al_5O_{12}$. *Solid State Commun.* **74**, 17–20, 10.1016/0038-1098(90)90201-L (1990).

235. Kornienko, A. A., Kaminskii, A. A. & Dunina, E. B. Dependence of the line strength of f–f transitions on the manifold energy. II. analysis of Pr^{3+} in $KPrP_4O_{12}$. *Phys. Status Solidi B Basic Res.* **157**, 267–273, https://doi.org/10.1002/pssb.2221570127 (1990).

236. Remillieux, A. *et al.* Upconversion mechanisms of a praseodymium-doped fluoride fibre amplifier. *J. Phys. D Appl. Phys.* **29**, 963–974, 10.1088/0022-3727/29/4/004 (1996).

237. Binnemans, K. *et al.* Absorption and magnetic circular dichroism spectra of praseodymium doped fluorozirconate (ZBLAN) glass. *J. Alloy. Compd.* **250**, 321–325, 10.1016/S0925-8388(96)02723-5 (1997).

238. Subramanyam Naidu, K. & Buddhudu, S. Fluorescence properties of Pr^{3+}-doped $(NaPO_3)_6$-$BaCl_2$-$ZnCl_2$-RF glasses. *J. Mater. Sci. Lett.* **11**, 386–389, 10.1007/BF00728717 (1992).

239. Hirao, K., Higuchi, M. & Soga, N. Upconversion mechanism of Pr^{3+} -doped fluoride fiber glass. *J. Lumin.* **60-61**, 115–118, 10.1016/0022-2313(94)90108-2 (1994).

240. Adam, J.-L., Rigout, N., Denoue, E., Smektala, F. & Lucas, J. Optical properties of Ba-In-Ga-based fluoride glasses for amplification at 1.3 μm. In Digonnet, M. J. F. & Snitzer, E. (eds.) *Fiber Laser Sources and Amplifiers III*, 10.1117/12.134980 (SPIE, 1992).

241. Amaranath, G. *et al.* Spectroscopic properties of Pr^{3+}-doped multicomponent fluoride glasses. *Mater. Res. Bull.* **25**, 1317–1323, 10.1016/0025-5408(90)90091-F (1990).

242. Seeber, W., Downing, E. A., Hesselink, L., Fejer, M. M. & Ehrt, D. Pr^{3+}-doped fluoride glasses. *J. Non Cryst. Solids* **189**, 218–226, 10.1016/0022-3093(95)00241-3 (1995).

243. Mazurak, Z., Łukowiak, E., Jeżowska-Trzebiatowska, B., Schultze, D. & Waligóra, C. Absorption and fluorescence intensity analysis of Pr^{3+} in $LiPrP_4O_{12}$ crystal. *J. Phys. Chem. Solids* **45**, 487–493, 10.1016/0022-3697(84)90084-2 (1984).

244. Simons, D. R., Faber, A. J. & de Waal, H. Pr^{3+}-doped GeS_x-based glasses for fiber amplifiers at 13 μm. *Opt. Lett.* **20**, 468, 10.1364/OL.20.000468 (1995).

245. Lakshman, S. V. J. & Buddhudu, S. Optical absorption spectrum of $PrCl_3$ complexes in solution. *J. Phys. Chem. Solids* **43**, 849–861, 10.1016/0022-3697(82)90034-8 (1982).

246. Tandon, S. P. & Mehta, P. C. Spectral intensities of some Pr^{3+} β-diketonates. *J. Chem. Phys.* **52**, 4313–4315, 10.1063/1.1673647 (1970).

247. Zhang, G., Ying, X., Yao, L., Chen, T. & Chen, H. Spectroscopic investigation of Pr^{3+} luminescence in $Sr_xBa_{1x}Nb_2O_6$ crystal. *J. Lumin.* **59**, 315–320, 10.1016/0022-2313(94)90058-2 (1994).

248. Hewak, D. W. *et al.* Quantum-efficiency of praseodymium doped Ga:La:S glass for 1.3 μm optical fibre amplifiers. *IEEE Photonics Technol. Lett.* **6**, 609–612, 10.1109/68.285556 (1994).

249. Wei, K., Machewirth, D. P., Wenzel, J., Snitzer, E. & Sigel, G. H., Jr. Pr^{3+}-doped GeGaS glasses for 1.3 μm optical fiber amplifiers. *J. Non Cryst. Solids* **182**, 257–261, 10.1016/0022-3093(94)00513-3 (1995).

250. Kaminskii, A. A. *et al.* Spectroscopy of a new laser garnet $Lu_3Sc_2Ga_3O_{12}$:Nd^{3+}. intensity luminescence characteristics, stimulated emission, and full set of squared reduced-matrix elements $|\langle\|U(t)\|\rangle|^2$ for Nd^{3+} ions. *Phys. Status Solidi A Appl. Res.* **141**, 471–494, 10.1002/pssa.2211410228 (1994).

251. Stokowski, S. E., Saroyan, R. A. & Weber, M. J. *Nd-doped laser glass spectroscopic and physical properties* (Office of Scientific and Technical Information (OSTI), 2004).

252. Orera, V. M., Trinkler, L. E., Merino, R. I. & Larrea, A. The optical properties of the Nd^{3+} ion in $NdGaO_3$ and $LaGaO_3$:Nd: temperature and concentration dependence. *J. Phys. Condens. Matter* **7**, 9657–9673, 10.1088/0953-8984/7/49/027 (1995).

253. Ryan, J. R. & Beach, R. Optical absorption and stimulated emission of neodymium in yttrium lithium fluoride. *J. Opt. Soc. Am. B* **9**, 1883, 10.1364/JOSAB.9.001883 (1992).

254. Kaminskii, A. A. & Li, L. Analysis of spectral line intensities of TR^{3+} ions in crystal systems. *Phys. Status Solidi A Appl. Res.* **26**, 593–598, 10.1002/pssa.2210260224 (1974).

255. Allik, T. H., Morrison, C. A., Gruber, J. B. & Kokta, M. R. Crystallography, spectroscopic analysis, and lasing properties of Nd^{3+}:$Y_3Sc_2Al_3O_{12}$. *Phys. Rev. B Condens. Matter* **41**, 21–30, 10.1103/PhysRevB.41.21 (1990).

256. Payne, S. A. *et al.* Spectroscopy and gain measurements of Nd^{3+} in SrF_2 and other fluorite-structure hosts. *J. Opt. Soc. Am. B* **8**, 726, 10.1364/JOSAB.8.000726 (1991).

257. Allik, T. H. *et al.* Preparation, structure, and spectroscopic properties of Nd^{3+}:$La_{1x}Lu_{x3}[Lu_{1y}Ga_y]_2Ga_3O_{12}$ crystals. *Phys. Rev. B Condens. Matter* **37**, 9129–9139, 10.1103/PhysRevB.37.9129 (1988).

258. Kaminskii, A. A., Mironov, V. S., Bagaev, S. N., Boulon, G. & Djeu, N. Strong ultraviolet and visible radiative channels of Nd^{3+}-doped insulating fluoride crystals. a new laser potentiality. *Phys. Status Solidi B Basic Res.* **185**, 487–504, 10.1002/pssb.2221850220 (1994).

259. Allik, T. H. *et al.* Crystal growth, spectroscopy, and laser performance of Nd^{3+}:KYF_4. *J. Opt. Soc. Am. B* **10**, 633, 10.1364/JOSAB.10.000633 (1993).

260. Sardar, D. K., Velarde-Montecinos, R. C. & Vizcarra, S. Spectroscopic properties of Nd^{3+} in CaF_2. *Phys. Status Solidi A Appl. Res.* **136**, 555–560, 10.1002/pssa.2211360228 (1993).

261. Tesar, A. *et al.* Optical properties and laser parameters of Nd^{3+}-doped flouride glasses. *Opt. Mater. (Amst.)* **1**, 217–234, 10.1016/0925-3467(92)90030-Q (1992).

262. Kaminskii, A. A., Mill, B. V., Butashin, A. V., Belokoneva, E. L. & Kurbanov, K. Germanates with $NdAlGe_2O_7$-type structure. synthesis, crystal structure, absorption-luminescence properties, and stimulated emission of their activator, Nd^{3+} ions. *Phys. Status Solidi A Appl. Res.* **103**, 575–592, 10.1002/pssa.2211030231 (1987).

263. Kaminskii, A. A. *et al.* Spectroscopy and laser action of anisotropic single-centered $LiKYF_5$: Nd^{3+} crystals grown by the hydrothermal method. *Phys. Status Solidi A Appl. Res.* **145**, 177–195, 10.1002/pssa.2211450117 (1994).

264. Weber, M. J. & Varitimos, T. E. Optical spectra and intensities of Nd^{3+} in $YAlO_3$. *J. Appl. Phys.* **42**, 4996–5005, 10.1063/1.1659885 (1971).

265. Sardar, D. K. & Stubblefield, S. C. Spectroscopic characterization of Nd^{3+} :BAMGAR crystal. *Phys. Status Solidi A Appl. Res.* **152**, 549–554, 10.1002/pssa.2211520223 (1995).

266. Azkargorta, J. *et al.* Spectroscopic and laser properties of Nd^{3+} in BIGaZLuTMn fluoride glass. *IEEE J. Quantum Electron.* **30**, 1862–1867, 10.1109/3.301650 (1994).

267. Kaminskii, A. A., Petrosyan, A. G., Markosyan, A. A. & Shironyan, G. O. Bridgman growth and stimulated-emission spectroscopy of orthorhombic $LuAlOs_3$ single crystals doped with Nd^{3+} and Pr^{3+} ions. *Phys. Status Solidi A Appl. Res.* **125**, 353–361, 10.1002/pssa.2211250133 (1991).

268. Bünzli, J.-C. G. & Vuckovic, M. M. Solvation of neodymium(III) perchlorate and nitrate in organic solvents as determined by spectroscopic measurements. *Inorganica Chim. Acta* **95**, 105–112, 10.1016/S0020-1693(00)87373-9 (1984).

269. Elejalde, M. J., Balda, R., Fernández, J., Macho, E. & Adam, J. L. Optical properties of Cr^{3+} and Nd^{3+} in singly- and doubly-doped barium-indium-gallium-based fluoride glass investigated by time-resolved laser spectroscopy. *Phys. Rev. B Condens. Matter* **46**, 5169–5182, 10.1103/PhysRevB.46.5169 (1992).

270. Binnemans, K., Van Deun, R., Görller-Walrand, C. & Adam, J. L. Optical properties of Nd^{3+}-doped fluorophosphate glasses. *J. Alloy. Compd.* **275-277**, 455–460, 10.1016/S0925-8388(98)00367-3 (1998).

271. Kaminskii, A. A. *et al.* Pure and Nd^{3+}-doped $Ca_3Ga_2Ge_4O_{14}$ and $Sr_3Ga_2Ge_4O_{14}$ single crystals, their structure, optical, spectral luminescence, electromechanical properties, and stimulated emission. *Phys. Status Solidi A Appl. Res.* **86**, 345–362, 10.1002/pssa.2210860139 (1984).

272. Lucas, J. *et al.* Preparation and optical properties of neodymium fluorozirconate glasses. *J. Non Cryst. Solids* **27**, 273–283, 10.1016/0022-3093(78)90130-8 (1978).

273. Balda, R., Fernandez, J., Mendioroz, A., Adams, J. L. & Boulard, B. Temperature-dependent concentration quenching of Nd^{3+} fluorescence in fluoride glasses. *J. Phys. Condens. Matter* **6**, 913–924, 10.1088/0953-8984/6/4/011 (1994).

274. Nageno, Y., Takebe, H. & Morinaga, K. Correlation between radiative transition probabilities of Nd^{3+} and composition in silicate, borate, and phosphate glasses. *J. Am. Ceram. Soc.* **76**, 3081–3086, 10.1111/j.1151-2916.1993.tb06612.x (1993).

275. Annapurna, K., Hanumanthu, M. & Buddhudu, S. Fluorescence properties of Nd^{3+} -doped InF_3 based optical glasses. *Spectrochim. Acta A* **48**, 791–797, 10.1016/0584-8539(92)80073-6 (1992).

276. Huang, Y., Tu, C., Luo, Z. & Chen, G. Spectra and intensity parameters of $Li_6Y(BO_3)_3$:Nd^{3+} laser crystal. *Opt. Commun.* **92**, 57–60, 10.1016/0030-4018(92)90218-G (1992).

277. Mondry, A. & Starynowicz, P. Optical spectroscopy and structure of neodymium complexes with 2,6-pyridine-dicarboxylic acid in solution and single crystal at room and low temperatures. *J. Alloy. Compd.* **225**, 367–371, 10.1016/0925-8388(94)07041-5 (1995).

278. Petrin, R. R. *et al.* Spectroscopy and laser operation of Nd:ZBAN glass. *IEEE J. Quantum Electron.* **27**, 1031–1038, 10.1109/3.83338 (1991).

279. Devi, A. R. & Jayasankar, C. K. Optical properties of Nd^{3+} ions in lithium borate glasses. *Mater. Chem. Phys.* **42**, 106–119, 10.1016/0254-0584(95)01564-7 (1995).

280. Naidu, K. S. & Buddhudu, S. Absorption properties of Nd^{3+}-doped $(NaPO_3)_6$-$BaCl_2$-$ZnCl_2$-RCl glasses. *J. Quant. Spectrosc. Radiat. Transf.* **47**, 515–519, 10.1016/0022-4073(92)90110-P (1992).

281. Carnall, W. T., Beitz, J. V., Crosswhite, H., Rajnak, K. & Mann, J. B. *Spectroscopic properties of the f-elements in compounds and solutions* (Springer Netherlands, Dordrecht, 1983).

282. Weber, M. J., Ziegler, D. C. & Angell, C. A. Tailoring stimulated emission cross sections of Nd^{3+} laser glass: Observation of large cross sections for $BiCl_3$ glasses. *J. Appl. Phys.* **53**, 4344–4350, 10.1007/978-94-009-7175-2_9 (1982).

283. Balda, R., Fernández, J., de Pablos A, Fdez-Navarro, J. M. & Arriandiaga, M. A. Temperature-dependent concentration quenching and site-dependent effects of Nd^{3+} fluorescence in fluorophosphate glasses. *Phys. Rev. B Condens. Matter* **53**, 5181–5189, 10.1103/PhysRevB.53.5181 (1996).

284. Kaminskii, A. A., Silvestrova, I. M., Sarkisov, S. E. & Denisenko, G. A. Investigation of trigonal $(La_{1\text{-}x}Nd_x)_3Ga_5SiO_{14}$ crystals. II. spectral laser and electromechanical properties. *Phys. Status Solidi A Appl. Res.* **80**, 607–620, 10.1002/pssa.2210800225 (1983).

285. Weber, M. J. & Almeida, R. M. Large stimulated emission cross section of Nd^{3+} in chlorophosphate glass. *J. Non Cryst. Solids* **43**, 99–104, 10.1016/0022-3093(81)90175-7 (1981).

286. Ray Bullock, S., Reddy, B. R., Pope, C. L. & Nash-Stevenson, S. K. Yellow to violet energy upconversion in Nd^{3+} doped oxide glass. *J. Non Cryst. Solids* **212**, 85–88, 10.1016/S0022-3093(97)00087-2 (1997).

287. Surana, S. S. L., Singh, M. & Misra, S. N. Intensity analysis of transitions and energy interaction parameters in studies of the structure of lanthanide haloacetates in solutions. *J. Inorg. Nucl. Chem.* **42**, 61–65, 10.1016/0022-1902(80)80044-3 (1980).

288. Bukietyńska, K. & Radomska, B. Spectral intensity analysis of the Dy^{3+}-$POCl_3$-$ZrCl_4$ system. *Chem. Phys. Lett.* **79**, 162–164, 10.1016/0009-2614(81)85310-9 (1981).

289. Devlin, M. T., Stephens, E. M. & Richardson, F. S. Comparison of electric-dipole intensity parameters for a series of structurally related neodymium, holmium, and erbium complexes in aqueous solution. theory and experiment. *Inorg. Chem.* **27**, 1517–1524, 10.1021/ic00282a003 (1988).

290. Rukmini, E. & Jayasankar, C. K. Spectroscopic properties of Ho^{3+} ions in zinc borosulphate glasses and comparative energy level analyses of Ho^{3+} ions in various glasses. *Opt. Mater. (Amst.)* **4**, 529–546, 10.1016/0925-3467(94)00125-1 (1995).

291. Csöregh, I. *et al.* Crystal structure, absorption, and fluorescence spectra of lanthanoid glutamate perchlorate nonahydrates, $Ln_2(C_5H_8NO_4)_2(ClO_4)_4.9H_2O$. *Acta Chem. Scand.* **43**, 735–747, 10.3891/acta.chem.scand.43-0735 (1989).

292. Cases, R., Chamarro, M. A., Alcala, R. & Rodriguez, V. D. Optical properties of Nd^{3+} and Dy^{3+} ions in ZnF_2-CdF_2 based glasses. *J. Lumin.* **48-49**, 509–514, 10.1016/0022-2313(91)90181-T (1991).

293. Hormadaly, J. & Reisfeld, R. Intensity parameters and laser analysis of Pr^{3+} and Dy^{3+} in oxide glasses. *J. Non Cryst. Solids* **30**, 337–348, 10.1016/0022-3093(79)90171-6 (1979).

294. Legendziewicz, J., Oczko, G. & Keller, B. Absorption spectra of dysprosium compounds in nonaqueous solutions. spectral intensity analysis. *Polyhedron* **3**, 161–168, 10.1016/S0277-5387(00)88046-8 (1984).

295. Gschneidner, K. A., Jr & Eyring, L. *Handbook on the Physics and Chemistry of Rare Earths Volume 28* (Elsevier, 2000).

296. Yang, J. *et al.* Spectroscopic and yellow laser features of Dy^{3+}:$Y_3Al_5O_{12}$ single crystals. *J. Inorg. Mater.* **38**, 350, 10.15541/jim20220386 (2023).

Acknowledgements

This work was supported by the Charles University (SVV–2024–260720, GA UK No. 662220). Besides that, authors would like to thank Lukas Strizik for valuable comments and discussion. Special thanks belong to Brian M. Walsh for his long-lasting and significant contribution to the field of RE ions spectroscopy and methodology of JO calculations which was an important factor in the development of this work.

Author contributions statement

All authors contributed equally to this work. J.H.: conceptualization, methodology, software, validation, formal analysis, investigation, visualization, supervision, funding aquisition and writing original draft, P.V. methodology, validation, formal analysis, visualization, investigation and writing - Review and editing; R.K. methodology, software, validation, formal analysis, visualization and writing - Review and editing. All authors reviewed the manuscript.

Competing interest

The authors declare no competing interests.

Additional information

Correspondence and request for materials should be addressed to J. Hrabovsky. Updated software documentation is available at Luminescence, optics and magneto-optics software (LOMS) webpage https://www.LOMS.cz/ as well as the GUI of the software itself.